Geochemistry Geophysics Geosystems G3

Article
Volume 13, Number 3
31 March 2012
Q03024, doi:10.1029/2011GC003902
ISSN: 1525-2027

Published by AGU and the Geochemical Society

Global variations in H_2O/Ce: 1. Slab surface temperatures beneath volcanic arcs

Lauren B. Cooper
Department of Mineralogy, University of Geneva, CH-1205 Geneva, Switzerland (lauren.cooper@erdw.ethz.ch)

Institute for Geochemistry and Petrology, ETH-Zurich, CH-8029 Zurich, Switzerland

Lamont-Doherty Earth Observatory, Columbia University, Palisades, New York 10964, USA

Daniel M. Ruscitto
Department of Earth and Environmental Sciences, Rensselaer Polytechnic Institute, Troy, New York 12180, USA

Terry Plank
Lamont-Doherty Earth Observatory, Columbia University, Palisades, New York 10964, USA

Paul J. Wallace
Department of Geological Sciences, University of Oregon, Eugene, Oregon 97403, USA

Ellen M. Syracuse
Department of Geoscience, University of Wisconsin-Madison, Madison, Wisconsin 53706, USA

Craig E. Manning
Department of Earth and Space Sciences, University of California, Los Angeles, California 90095, USA

[1] We have calculated slab fluid temperatures for 51 volcanoes in 10 subduction zones using the newly developed H_2O/Ce thermometer. The slab fluid compositions were calculated from arc eruptives, using melt inclusion-based H_2O contents, and were corrected for background mantle contributions. The temperatures, adjusted to *h*, the vertical depth to the slab beneath the volcanic arc, range from ~730 to 900°C and agree well (within 30°C on average for each arc) with sub-arc slab surface temperatures predicted by recent thermal models. The coherence between slab model and surface observation implies predominantly vertical transport of fluids within the mantle wedge. Slab surface temperatures are well reconciled with the thermal parameter (the product of slab age and vertical descent rate) and *h*. Arcs with shallow *h* (~80 to 100 km) yield a larger range in slab surface temperature (up to ~200°C between volcanoes) and more variable magma compositions than arcs with greater *h* (~120 to 180 km). This diversity is consistent with coupling of the subducting slab and mantle wedge, and subsequent rapid slab heating, at ~80 km. Slab surface temperatures at or warmer than the H_2O-saturated solidus suggest that melting at the slab surface is common beneath volcanic arcs. Our results imply that hydrous melts or solute-rich supercritical fluids, and not H_2O-rich aqueous fluids, are thus the agents of mass transport to the mantle wedge.

Copyright 2012 by the American Geophysical Union

Components: 14,400 words, 11 figures, 1 table.

Keywords: geothermometer; slab fluid temperature; sub-arc slab surface temperature.

Index Terms: 1031 Geochemistry: Subduction zone processes (3060, 3613, 8170, 8413); 3652 Mineralogy and Petrology: Pressure-temperature-time paths.

Received 29 September 2011; **Revised** 10 February 2012; **Accepted** 12 February 2012; **Published** 31 March 2012.

Cooper, L. B., D. M. Ruscitto, T. Plank, P. J. Wallace, E. M. Syracuse, and C. E. Manning (2012), Global variations in H_2O/Ce: 1. Slab surface temperatures beneath volcanic arcs, *Geochem. Geophys. Geosyst.*, *13*, Q03024, doi:10.1029/2011GC003902.

1. Introduction

[2] Subduction zones are tectonic boundaries where oceanic crust and overlying sediment are thrust downward into the mantle. The fate of volatiles contained within the subducting slab is mainly dependent upon the slab's pressure-temperature (*P-T*) path and how this influences the stability of volatile-bearing minerals [e.g., *Hacker*, 2008; *van Keken et al.*, 2011]. Of particular interest in this process are the reactions that occur in the slab beneath volcanic arcs (~90 to 120 km on average [*England et al.*, 2004; *Syracuse and Abers*, 2006]), as they initiate another process responsible for recycling volatiles to the surface of the Earth. This study focuses on this critical zone in the slab beneath the arc.

[3] The thermal structure of subducting slabs (Figure 1) determines both the quantity and composition of slab fluids released into the mantle wedge. Warm slabs may drive efficient dehydration, and as a consequence, subducted volatiles may be returned to the surface via arc volcanism. On the other hand, cool slabs may inhibit dehydration reactions, and volatiles could be retained to greater depths where they may hydrate the deep Earth [e.g., *Ohtani et al.*, 2004; *Hirschmann et al.*, 2006]. Thus, each subduction zone may recycle volatiles with different efficiency depending primarily on its thermal structure [*van Keken et al.*, 2011].

[4] The solute content and trace element (TE) signature of slab fluids are also controlled by slab thermal structure. Slab fluids are predominantly aqueous and poor in many tracers, like the rare earth elements (REE), at temperatures below the wet solidus (~700°C at 3 GPa [*Manning*, 2004; *Schmidt et al.*, 2004; *Hermann and Spandler*, 2008]), and composed of hydrous melts rich in many tracers at higher temperatures [*Kessel et al.*, 2005a; *Hermann et al.*, 2006; *Hermann and Spandler*, 2008]. When pressure is greater than the 2nd critical end-point on the wet solidus of a slab lithology (as of yet not well determined, but likely >2.5 GPa [*Schmidt et al.*, 2004; *Kessel et al.*, 2005b; *Klimm et al.*, 2008, *Mibe et al.*, 2011]), slab fluids may be supercritical with complete miscibility between aqueous fluids and hydrous melts [*Manning*, 2004]. In this region, there may still be a rapid change in solute proportions, not as abrupt, but comparable to the changes that occur at the solidus [*Manning*, 2004; *Hermann et al.*, 2006]. The transport properties of these fluids, trace element partition coefficients, and mineral solubilities are all a strong function of solute content, which scales strongly with temperature [*Hermann et al.*, 2006].

[5] Arc magmas derive in part from the fluids that exit the slab and drive melting in the mantle, and inherit their unusual trace element signatures from them. Arc magmas are the primary products of the subduction zone; they build the continental crust, and their geochemical compositions are the principle tools we use to infer the conditions under which the slab dehydrates. This is possible only if we understand how minerals and fluids interact chemically in the subduction zone, and laboratory experiments yield wide-ranging results. Experimental studies by *Johnson and Plank* [1999], *Kessel et al.* [2005a, 2005b], *Hermann and Spandler* [2008], *Klimm et al.* [2008], *Hermann and Rubatto* [2009], and *Skora and Blundy* [2010a] have used synthetic starting compositions engineered to approximate oceanic crust and sediment, and from them, generated fluids that change composition as a function of *P* and *T*. The interpretation of these experimental results with respect to the geochemical composition of specific arcs has led collectively to a wide range of inferred slab fluid temperatures, from ~700 to 1,000°C [*Keppler*, 1996; *McDade et al.*, 2003; *George et al.*, 2005; *Portnyagin et al.*, 2007; *Johnson et al.*, 2009; *Ruscitto et al.*, 2010]. Moreover, the view from one element might contrast with

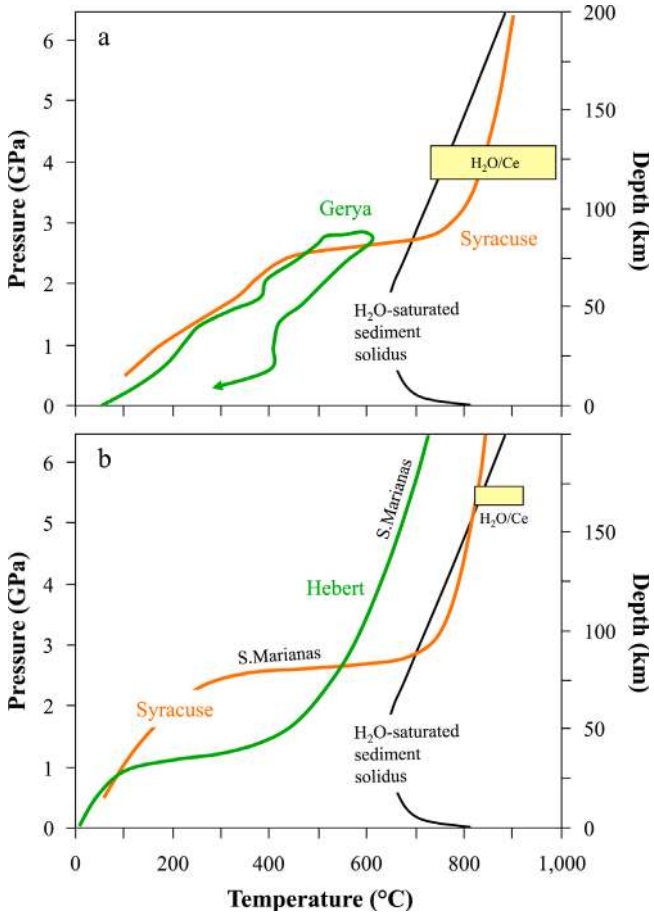

Figure 1. Comparison of numerical models of slab surface *P-T* paths. (a) Green line is the *P-T* path for material in the subduction channel that detaches and then rises buoyantly in the mantle (HYAD model from *Gerya and Stoeckhert* [2006], for a 40 Ma slab and 30 mm/yr convergence rate). Orange line is the D80 model from *Syracuse et al.* [2010] (see Table 1 footnotes for details) for North Vanuatu, which has comparable subducting parameters (39.6 mm/yr and a 44 Ma slab). Yellow box represents the total range in slab fluid temperatures at 4 GPa for individual volcanoes, calculated from melt inclusions using the H_2O/Ce thermometer of *Plank et al.* [2009] given in equation (1) (see Table 1). (b) Models for the S. Mariana slab, from *Hebert et al.* [2009] (green line) and *Syracuse et al.* [2010] (orange line). Yellow box represents the H_2O/Ce temperature (±50°C) for the Mariana arc, adjusted for *h*, the depth of the slab beneath the arc [from *Syracuse et al.*, 2010]. For both panels, the H_2O-saturated sediment solidus is shown for reference (black line; based on experiments of *Hermann and Spandler* [2008]).

that from another. For example, B is generally considered to be lost from the slab at relatively low temperatures (<550°C) while Th is thought to be lost at relatively high temperatures (>750°C, above the wet sediment solidus). How do we interpret arcs with both B and Th enrichment [*Elliott*, 2003]? Do multiple fluids from different thermal regions of the slab mix [*Elliott et al.*, 1997]? Or does slab material itself mix and undergo a range of metamorphic reactions [*King et al.*, 2006]? How much material is dragged down with the slab [*Tatsumi*, 1986; *Hebert et al.*, 2009] versus buoyantly detached from the slab [*Gerya and Yuen*, 2003; *Currie et al.*, 2007]?

[6] Another major unanswered question in plate tectonics is why volcanic arcs form where they do, above a narrow but significant range of depths to the slabs, from ~60 to 200 km [*England et al.*, 2004; *Syracuse and Abers*, 2006]. Ideas fall into three groups – those that emphasize slab, mantle, or upper-plate control. Early proposals for slab control focused on critical dehydration reactions in or along the slab as the ultimate source of arc volcanism [e.g., *Tatsumi*, 1986]; more recent ideas have focused on the total slab flux of volatiles at any given depth [*Rüpke et al.*, 2002] or linkages between slab seismic velocity structure and the location of the mantle

melting region [*Syracuse et al.*, 2008]. Another group of models postulates instead that a critical reaction or critical isotherm in the mantle, modulated by focused fluid or melt flow, controls the locus of volcanism at the surface [*Davies and Stevenson*, 1992; *Schmidt and Poli*, 1998; *England and Wilkins*, 2004; *Syracuse and Abers*, 2006; *Grove et al.*, 2009; *England and Katz*, 2010]. Finally, upper plate structure or stress regime may control the final pathways of magma to the surface [*Kay et al.*, 1982; *MacKenzie et al.*, 2008]. Despite long-standing interest and no lack of ideas, it is still not clear what controls the location of volcanic arcs worldwide. One problem has been the lack of constraints on the thermal structure in subduction zones, which determines the magnitude and location of fluid flux from the slab.

[7] Independent constraints on slab thermal structure come from numerical and analog geodynamic models. Current models, however, conflict in their predictions as to whether subducting material will experience sub-solidus, solidus, supersolidus, or supercritical reactions at sub-arc depths (Figure 1). Uncertainties in the depth of slab-mantle wedge coupling, mantle rheology, and slab geometry have yielded wide variations in the estimates of sub-arc slab surface temperatures (SASSTs). For example, thermal models from *England and Wilkins* [2004], *Gerya and Stoeckhert* [2006], *Arcay et al.* [2007], and *Iwamori* [2007] predicted SASSTs uniformly <700°C. In contrast, *Kincaid and Sacks* [1997], *van Keken et al.* [2002], *Kelemen et al.* [2003], and *Syracuse et al.* [2010] predicted SASSTs between ~700 and 950°C. These latter results agree with those from the scaled analog (tank) models from *Kincaid and Griffiths* [2004] — one of few models to incorporate three-dimensions. Figure 1 compares a few models with comparable input parameters. *Gerya and Stoeckhert* [2006] incorporate multiple weak and buoyant materials that lead to the development of a subduction channel and significant upward flow of material back toward the surface. While these models are useful for envisioning how ultra-high pressure rocks may be rapidly exhumed, they predict uniformly cool temperatures in the subduction channel and mantle wedge [*Castro and Gerya*, 2008]. *Hebert and Gurnis* [2010] incorporate mantle hydration and melting, leading to a low viscosity channel above the slab surface that perturbs flow, warming the shallow slab but leaving the deeper slab cool, despite a very hot input mantle (1,500°C). Thus, current models incorporate complex behavior, and yet predict slab surface temperatures that differ by hundreds of degrees at the same depth.

[8] With such disparate models and such varied interpretation of arc magmas, what is needed are new constraints and a confluence of model and observation. Two recent advances offer such opportunity. One is the development of new geothermometers. *Plank et al.* [2009] review the topic and present a new potential slab fluid thermometer based on the ratio of H_2O/Ce, using H_2O measured in mafic arc melt inclusions. The other is a new study by *Syracuse et al.* [2010] that provides self-consistent thermal models for each global subduction zone. Our goal is to compare the geothermometry results with the thermal models for several subduction zones that have magmatic H_2O data (e.g., Tonga, the Marianas, Kamchatka, the Aleutians, Cascadia, Mexico, Central America, and the Lesser Antilles; Figure 2), and which span a range of subduction parameters (e.g., depth to slab, slab age, and descent rate). This paper addresses three important questions: Do the data and models provide a coherent view of slab temperatures beneath arcs? Do we understand why some subduction zones seem to have higher SASSTs than others? How does slab thermal structure affect the locus of volcanism at the surface and the composition of magmas that erupt? Some additional questions are addressed by a companion paper [*Ruscitto et al.*, 2012]: Do other slab tracers correlate with inferred SASSTs? Do slab fluid compositions reconstructed from parental magmas vary between arcs characterized by different thermal regimes? Are volatile fluxes and recycling efficiencies estimated from arc volcanoes in agreement with what is expected from thermal models?

2. The H_2O/Ce Thermometer

[9] The traditional approach to inferring the temperature of slab dehydration reactions is to focus on a suite of trace elements in arc magmas (i.e., using a spider diagram or trace element ratios), and compare the observations to laboratory experiments that determine solid/fluid bulk partitioning as a function of temperature [e.g., *Brenan et al.*, 1995; *Keppler*, 1996; *Johnson and Plank*, 1999; *Kessel et al.*, 2005a; *Hermann and Rubatto*, 2009]. While such approaches have been valuable in identifying different kinds of components found in arc magmas (tagged as aqueous fluids, hydrous melts, or supercritical fluids [*Elliott et al.*, 1997; *Turner et al.*, 1996; *Straub et al.*, 2004; *Portnyagin et al.*, 2007]), they

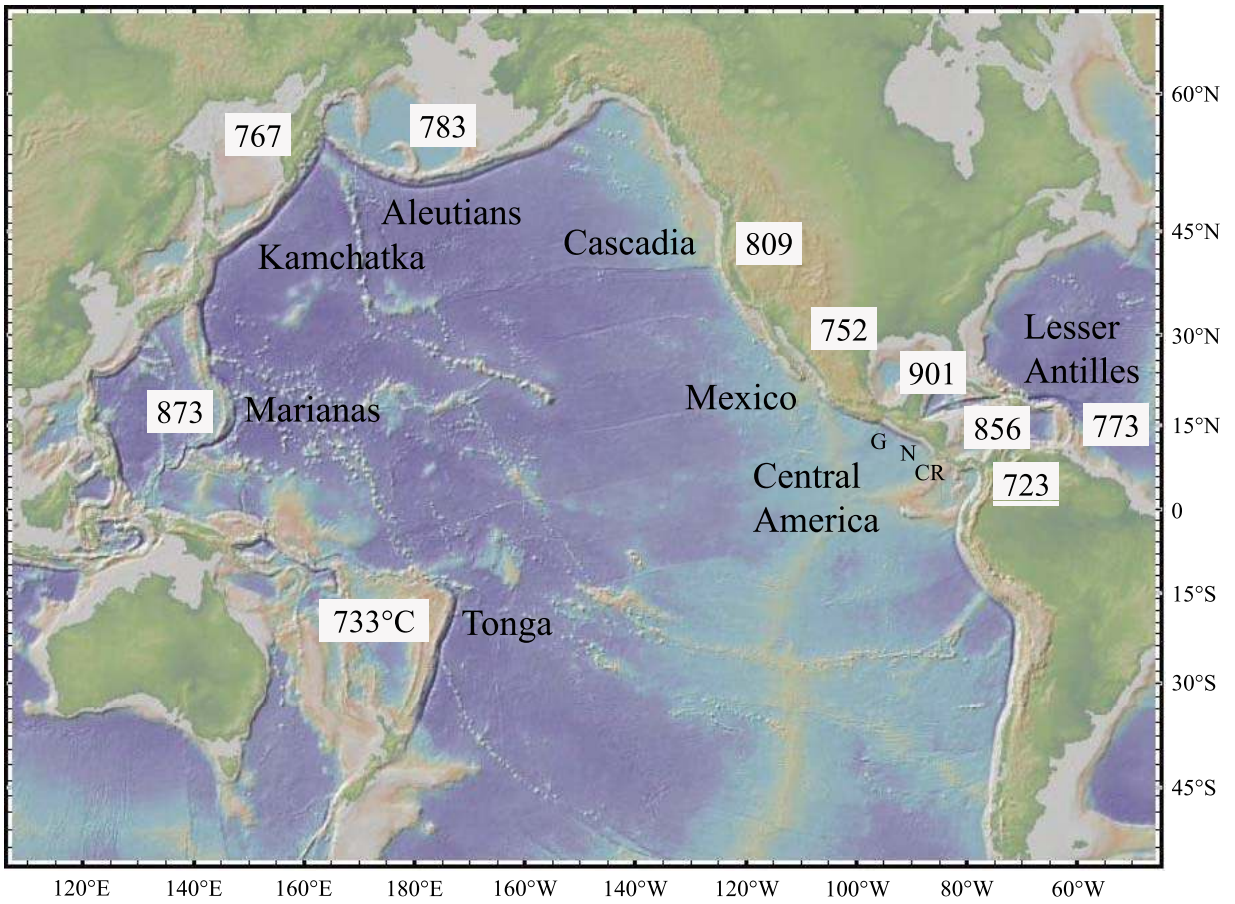

Figure 2. Location map (from GeoMapApp) of the subduction zones in this study. For Central America, volcanoes within the political boundaries of Guatemala, Nicaragua, and Costa Rica are distinguished, based on prior work which found large physical and geochemical variations along strike. Boxed numbers indicate slab surface temperatures beneath each arc (from Table 1), based on H_2O/Ce ratios measured in melt inclusions (H_2O) and the depth to slab beneath the arc (h) from *Syracuse et al.* [2010]. Temperatures generally increase with both h and thermal parameter (age * vertical descent rate).

are limited in their ability to constrain temperature with any accuracy. In fact, it is currently intractable to fully constrain the partitioning of most trace elements in slab fluids as a function of equilibration temperature, given the shear number of variables involved. For example, the fluid concentration of Sr at any given temperature requires knowing the compatibility of Sr in a multitude of minerals (e.g., feldspar, lawsonite, pyroxene, and apatite, among others), the proportions of these minerals within the system, the fluid fraction, and the bulk composition. This kind of information is rarely available at any temperature for even a single bulk composition. On the other hand, some trace elements may serve as major structural components in certain minerals (e.g., Zr in zircon, K in mica, Ti in rutile, and REE in monazite and allanite), and so their concentration in fluids will depend on the solubility of these minerals, which may be less dependent on bulk composition, the presence of other phases, or modal abundances. For example, the TiO_2 content of a rutile-saturated fluid will be fixed by rutile (TiO_2) solubility, thus simplifying greatly the problem of predicting fluid concentrations in multiphase assemblages. Several recent studies have determined the solubility of trace element-rich minerals at high temperature and high pressure [e.g., *Hayden and Watson*, 2007; *Antignano and Manning*, 2008; *Hermann and Spandler*, 2008; *Hermann and Rubatto*, 2009; *Skora and Blundy*, 2010a; *Tropper et al.*, 2011; *Hayden and Manning*, 2011], and this work has motivated a new class of geothermometers.

[10] Recently proposed fluid thermometers include K_2O/H_2O (based on the solubility of phengite [*Hermann and Spandler*, 2008]), light REE/Ti (based on the solubilities of allanite and rutile

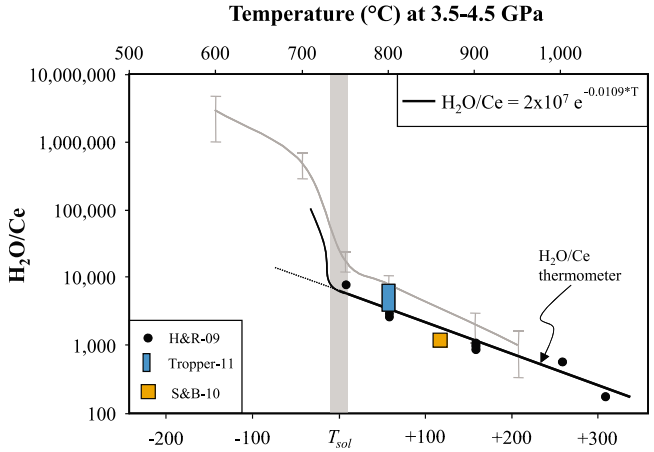

Figure 3. H_2O/Ce slab fluid thermometer, after *Plank et al.* [2009]. H_2O/Ce ratios are from experimentally synthesized high pressure fluids and melts, as a function of temperature above the H_2O-saturated sediment solidus (T_{sol}). Absolute temperatures are given along the top axis. Grey curve with error bar is fit to all experimental data (individual experiments not shown but given in the work of *Plank et al.* [2009]). Black line is the preferred thermometer, fit through sediment melting experiments of *Hermann and Rubatto* [2009], and relevant to the pressure range of 3.5 to 4.5 GPa. Equation (1) is only valid at temperatures above the H_2O-satuated solidus. Also shown are monazite-saturated aqueous fluids of *Tropper et al.* [2011] at X_{NaCl} = 0.1–0.2 (plotted at 800°C, even though the experiments were conducted at 1 GPa). Orange box is sediment melt at monazite-exhaustion from *Skora and Blundy* [2010a] for 7 wt% H_2O in the system (plotted at +110 above the solidus, as for their composition at 840°C and 3 GPa; and assuming a natural Ce/REE ratio of 0.4, as in the work of *Plank et al.* [2009]).

[*Klimm et al.*, 2008]), and H_2O/Ce (based on the solubility of allanite or monazite [*Plank et al.*, 2009] (Figure 3)). The H_2O/Ce ratio has the advantage that it varies by 4 orders of magnitude in fluids generated between ~600 and 1,000°C at 4 GPa (unlike light REE/Ti, which varies by only a factor of 10) and is readily resolved in arc magmas from background mantle values (unlike K_2O/H_2O, which overlaps in arc, mid-ocean ridge, and ocean island basalts). Moreover, H_2O/Ce has two further advantages as a thermometer: 1) it varies little in basalts from other tectonic settings (200 ± 100 [*Michael*, 1995; *Dixon et al.*, 2002]); and 2) it is minimally fractionated during partial melting in the mantle due to similar partitioning of H_2O and Ce in anhydrous peridotite [*Hauri et al.*, 2006]. We thus focus on the H_2O/Ce tool here.

[11] In detail, the inverse relationship between H_2O/Ce and temperature (Figure 3) stems from two independent thermometers that vary with temperature in opposite senses. The first is the variation in the concentration of H_2O in fluids (used here broadly to mean anything from aqueous fluid to hydrous melt to supercritical fluid) as a function of temperature, from >90% H_2O in low-temperature (<700°C) aqueous fluids to <20% H_2O in hydrous silicate melts or high-temperature supercritical fluids [*Manning*, 2004; *Kessel et al.*, 2005b; *Hermann and Spandler*, 2008] (Figure 4). The second relationship is based on the solubility of allanite and monazite, and their control on light REE abundances as a function of temperature [*Montel*, 1993; *Kessel et al.*, 2005a; *Klimm et al.*, 2008; *Hermann and Rubatto*, 2009]. The several orders of magnitude increase in the solubility of REE phases from ~600 to 1000°C, coupled with the factor of ~10 decline in H_2O concentration, means that the ratio of H_2O to light REE provides excellent sensitivity with respect to temperature.

[12] To simplify its application, *Plank et al.* [2009] normalized H_2O to a single light REE, Ce. The choice of Ce was motivated by the common use of the H_2O/Ce ratio in other kinds of settings. *Michael* [1995] first pointed out the near constancy of H_2O/Ce in mid-ocean ridge basalts (MORBs), which has been widely used as a constraint on the H_2O content of the upper mantle. Since then, *Dixon et al.* [2002], *Hauri et al.* [2006], and *Workman et al.* [2006] have extended its utility to ocean island basalts (OIBs) and deeper mantle processes. Given this well-developed background, it seemed natural to consider this ratio in arcs. Moreover, as discussed further below, the H_2O/Ce ratio of least-degassed arc magmas is uniformly higher than its restricted range in MORB and OIB. Potential drawbacks to using Ce are that it may occur in two oxidation

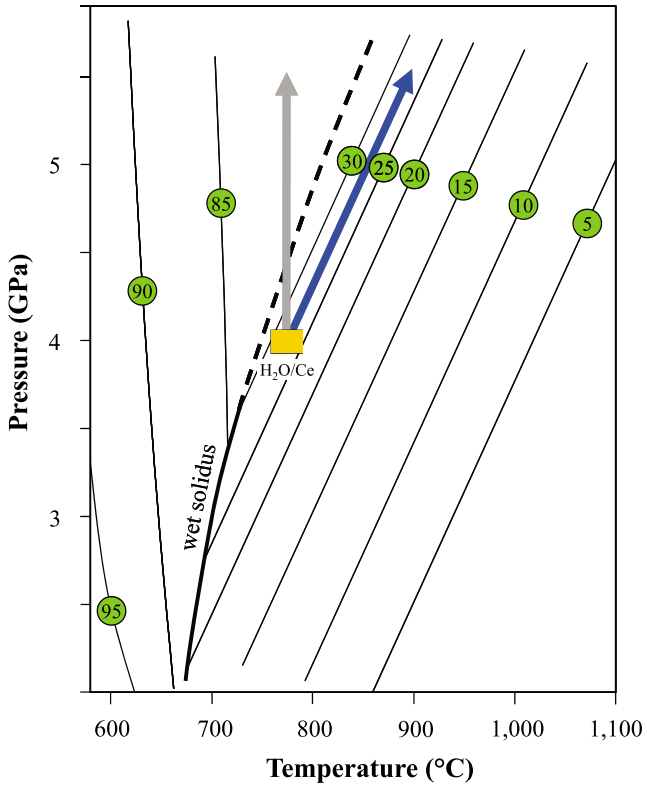

Figure 4. Extrapolation of the H_2O/Ce thermometer to different pressures, guided by H_2O-isopleths from *Hermann and Spandler* [2008] (contoured in wt% H_2O for aqueous fluids and melts; green circles). The H_2O/Ce thermometer given in equation (1) is calibrated at ~4.0 GPa. In order to apply the thermometer to different pressures, assumptions must be made as to how to extrapolate the H_2O/Ce temperatures. An isothermal pressure correction (gray arrow) would correspond to fluids with very different solute properties, and likely H_2O/Ce. Instead, H_2O/Ce temperatures are projected (blue arrow) along a *P-T* slope parallel to the H_2O-isopleths (~80°C/GPa or 2.5°C/km), which may be an adequate approximation as long as H_2O/Ce predicts temperatures within the supersolidus region (which they uniformly do). Water-isopleths and wet sediment solidus are based on experiments 2.5 to 4.5 GPa from *Hermann and Spandler* [2008]. The wet solidus is defined in their experiments up to 3.5 GPa, above which may lie the second critical end-point (somewhere along the dashed line).

states (+3 and +4) and its partition coefficient is not strictly identical to that of H_2O during mantle melting [*Hauri et al.*, 2006]. However, we find that H_2O/Ce is highly correlated to H_2O/La in arc eruptives (Pearson correlation coefficient of 0.99), demonstrating a minor role for oxidation on Ce contents. This is consistent with the small magnitude (≤10%) Ce anomalies observed in arc REE patterns [*Elliott et al.*, 1997]. Due to the similar overall partitioning between H_2O and all the light REE, we continue to express the slab fluid geothermometer in terms of H_2O/Ce because of its historical use in igneous geochemistry.

[13] The experimental predictions are dramatic for the variations in H_2O/Ce in slab fluids: from H_2O/Ce ratios on the order of 10^6 at low temperatures (~600°C, in nearly pure aqueous fluids), dropping to 10^3–10^4 at higher temperatures (~700 to 900°C, in the H_2O-present melting region; Figure 3). Based on this, and guided by the experiments of *Hermann and Rubatto* [2009], *Plank et al.* [2009] proposed a new geothermometer for slab fluids based on the near linear variation in ln(H_2O/Ce) with temperature above the H_2O-saturated sediment solidus at 4 ± 0.5 GPa:

$$\ln(H_2O/Ce) = 16.81 - 0.0109 * T_{4GPa} \quad (1)$$

where T_{4GPa} is the temperature (in °C) at 4 GPa. We envision the thermometer to pertain most to sediment melting because that is the lithology expected at the slab surface; however, the thermometer would also be applicable to the melting of metabasalt with allanite present [*Klimm et al.*, 2008; *Plank et al.*, 2009].

[14] Equation (1) is limited in its applicability to temperatures above the solidus, at pressures near

4 GPa, and requires the assumption that the mantle contributions to H_2O and Ce are small; however, these limitations can be overcome to facilitate its wider deployment. With respect to the solidus, Figure 3 illustrates that H_2O/Ce varies rapidly (10^4 to 10^5) in the near-solidus region. Thus, a different expression would be required to parameterize this part of the H_2O/Ce-temperature relationship. In practice, however, few arc basalts possess such high H_2O/Ce typical of solidus or sub-solidus temperatures. In the arcs examined in this study, only three volcanoes have H_2O/Ce greater than the nominal 4 GPa solidus value of ~7,000. In these cases the temperature can simply be fixed at the solidus, which we take here to be 730°C at 4 GPa (based on the experimental study of *Hermann and Spandler* [2008]). It is worth noting that this solidus temperature is the minimum reported in experimental studies at 4 GPa ([e.g., *Schmidt et al.*, 2004] report 780–850°C at 4 GPa), and significant variations are expected for different bulk and fluid compositions [e.g., *Thomsen and Schmidt*, 2008; *Tsuno and Dasgupta*, 2012]. Future studies may take into account solidus variations, as well as a new function to calibrate H_2O/Ce > 7,000.

[15] The pressure limitation arises because the calibration in equation (1) is strictly relevant to the narrow pressure range of 3.5 to 4.5 GPa [*Plank et al.*, 2009]. However, slab fluids may acquire their H_2O/Ce at a different pressure, so a pressure correction may be necessary (see section 3.3 for details about the correction and section 5.1 for the application). Finally, use of equation (1) to infer slab surface temperature requires that the H_2O/Ce ratio in arc magmas is set largely at the slab surface, with little subsequent contribution from the mantle or the crust. The potentially important role of the mantle can be assessed via correlations with other incompatible trace elements, such as Nb, and such a method is developed in a later section of this paper (section 3.2). Other limitations of the H_2O/Ce thermometer (i.e., the condition of allanite and monazite saturation; and the effects of fluid-melt miscibility, fluid-rock reaction in the mantle, and multiple fluids from the slab) are addressed in the supplement to the work of *Plank et al.* [2009].

[16] Since the development of the H_2O/Ce geothermometer, three studies have raised potential complications. One involves compositional controls on monazite solubility, independent of temperature. For example, *Tropper et al.* [2011] carried out experiments that demonstrate how dissolved NaCl substantially enhances Ce-monazite solubility in aqueous fluids, where X_{NaCl} of 0.1 to 0.5 results in a ten-fold decrease in H_2O/Ce at constant T. However, at intermediate salinities not uncommon to metamorphic settings (X_{NaCl} = 0.1 to 0.2), such fluids possess H_2O/Ce ratios similar to the melts used to calibrate the thermometer in the work of *Plank et al.* [2009] at 800°C (Figure 3). Moreover, the H_2O versus Cl systematics in most arc magmas are consistent with slab fluids similar to seawater in salinity, and thus X_{NaCl} even less than 0.1 (~0.05 for 3.5% NaCl brine [*Wallace*, 2005; *Ruscitto et al.*, 2012]). In their sediment melting experiments, *Skora and Blundy* [2010a] pointed out that both Th solid solutions in monazite (brabantite and huttonite) and total H_2O in the system may affect monazite solubility at constant temperature. Their recent work [*Skora and Blundy*, 2010b] also points to a trade-off between the activities of PO_4^{2-} and LREE in monazite-saturated melts, an effect that may lead to lower concentrations of REE in the melt for natural sediment systems with high PO_4^{2-}. The latter effect requires consideration of apatite-saturation within the context of the apatite content of natural sediments in order to quantify the effect on monazite solubility. Nonetheless, all of this work points to substantial effects on monazite solubility, driven by both fluid composition (Cl, PO_4^{2-}) or solid solutions (Th, other REE), that must be taken into account in refining an accurate H_2O/Ce thermometer. Future experiments are needed to develop such compositional parameterizations, but in this paper, we continue to exploit the large temperature dependence.

[17] The other concern is related to the basic premise of the thermometer — that slab fluids are saturated with allanite and/or monazite. *Plank et al.* [2009] used mass balance to predict that slab fluids will be allanite- or monazite-saturated in sediment up to ~950°C and 40% melting. However, if the sediments at the top of the slab are flushed with fluids derived from greater depths in the slab, then they can melt to large enough degrees to exhaust the REE phase even at lower temperatures. Based on their experimental results, *Skora and Blundy* [2010a] calculate monazite-out at ~780°C and 55% melting if sediment is flushed with 15 wt% H_2O. In this case, the REE will no longer be controlled by a REE phase, and H_2O could saturate the melts, rendering the H_2O/Ce thermometer inapplicable. For high fluid flushes (i.e., at high H_2O:rock ratios), H_2O/Ce could climb to very high values (>100,000) when Ce becomes dilute as H_2O is increasingly added. For example, a sediment with GLOSS Ce concentration of 57 ppm could yield a

fluid with H_2O/Ce of 100,000 if all the Ce were extracted into a fluid 5.7 times the mass of the sediment. Such high integrated fluid:rock ratios could be attained locally upon multiple episodes of fluid addition supplied by dehydration reactions occurring deeper in the slab (e.g., lawsonite and/or serpentine breakdown). Indeed, fluid addition after monazite exhaustion and LREE extraction could lead to H_2O/Ce approaching infinity. Such very high H_2O/Ce ratios are not observed in arc magmas, and so the system does not seem to reach this state of high fluid:rock ratio and/or fluid-addition after monazite exhaustion. On the other hand, the Th and La partitioning relationships determined by *Skora and Blundy* [2010a], which are complicated by non-Henrian behavior due to doping levels in experiments, predict Th-La fractionation in monazite-saturated melts, which violates the general lack of fractionation observed in arc magmas [*Plank*, 2005]. They conclude from this that slab fluids cannot be monazite-saturated, and that fluid flushing exhausts monazite. Thus, the requirements of both H_2O/Ce and Th/La provide tight constraints on the behavior of monazite in subducting sediments. It may be that melting at conditions near monazite-out will retain the temperature-dependence, while causing minimal fractionation of Th from La. This is apparently true at ~800°C, where *Skora and Blundy* [2010a] predict monazite-out for 7 to 15 wt% H_2O (Figure 3), but it remains to be seen for other conditions.

3. Methods

3.1. Arc Eruptive Sampling

[18] The purpose of this study was to apply the H_2O/Ce fluid thermometer to slab fluid compositions from 51 volcanoes in 10 subduction zones in order to test whether the estimated temperatures relate to those predicted from thermal models. The sources and treatment of the arc data are detailed in Text S1 in the auxiliary material and the data set is summarized in Table 1.[1] The data consist of melt inclusion-based H_2O concentrations measured by ion probe or infrared spectroscopy, and high-precision trace element compositions of erupted whole rocks (WRs), or in some cases, the melt inclusions themselves.

[19] Melt inclusions (MIs) are pockets of melt that become trapped within a phenocryst during crystallization. The strong pressure-dependence of volatile solubility in melts means that WRs and matrix glasses are highly degassed, while MIs may preserve pre-eruptive H_2O contents that approach those of the initial, undegassed magma [*Anderson*, 1979; *Sobolev and Chaussidon*, 1996; *Newman et al.*, 2000]. We used the maximum H_2O content measured in MIs from each volcano to represent the original H_2O content prior to ascent. Many processes (e.g., degassing of melt, diffusive exchange through crystals, CO_2 gas-fluxing, crustal contamination) can reduce H_2O and H_2O/Ce, and so temperatures calculated here are maxima. However, in many instances, coherent populations of melt inclusions trapped in near-primary olivine ($\geq Fo_{89}$) must reflect near-primary H_2O contents, as degassing of H_2O inevitably drives crystallization and magma evolution (see examples in the work of *Plank et al.* [2009]). To screen for the least contaminated and most primitive and undegassed magmatic compositions, we used only basalts and basaltic andesites, and most commonly MIs trapped in olivine hosts. We take our screened compositions to record primary elemental ratios from the mantle wedge, and assume that they have not been affected by crustal processes. Because the quality of trace element data is usually better for WRs than MIs, we primarily took Ce concentrations (and Nb concentrations, see section 3.2) from the analyses of the WR-hosts of the least-degassed MIs. Differences in Ce concentrations between WRs and MIs (generally 5 to 20%) have a small effect on the calculated temperatures due to the logarithmic nature of the H_2O/Ce fluid thermometer.

3.2. Determination of Slab Fluid Compositions via Mantle-Unmixing

[20] A component of the observed H_2O/Ce in arc eruptives must be due to contributions from the sub-arc mantle. The sub-arc mantle ranges from highly depleted to highly enriched in trace elements [e.g., *Pearce*, 2005; *Leeman et al.*, 2005; *Plank*, 2005; *Caulfield et al.*, 2008]. Could high H_2O/Ce simply reflect a mantle initially more depleted in Ce? While this makes intuitive sense, it is important to consider the full mixing problem, because both H_2O and Ce are being added from the slab to a mantle that contains both H_2O and Ce. This question can be answered by unmixing the mantle from the arc composition to reveal the H_2O/Ce ratio of the added slab fluid [e.g., *Portnyagin et al.*, 2007, *Ruscitto et al.*, 2010]. In carrying out this exercise, it is useful to consider an element that is minimally added in slab fluids, and like others [*Pearce et al.*, 2005], we take that to be Nb. Here, we normalize

[1]Auxiliary materials are available in the HTML. doi:10.1029/2011GC003902.

Table 1. Arc Eruptive and Slab Fluid Compositions and Temperatures

	Arc Eruptives									Slab Fluids				Geophys. Thermal Models		
	H_2O[a] (wt%)	K_2O[a] (wt%)	Ce[a] (ppm)	Nb[a] (ppm)	Nb/Ce (ppm/ppm	H_2O/Ce (ppm/ppm)	Temp. (H_2O/Ce)[b] (°C)	K_2O/H_2O (wt%/wt%)	Temp. (K_2O/H_2O)[c] (°C)	H_2O/Ce; Projected From H-DMM[d] (ppm/ppm)	H_2O/Ce; Projected From E-MORB[d] (ppm/ppm)	Temp. (H_2O/Ce)[b] (°C)	Temp. (Corr.)[e] (°C)	Temp. (D80)[f] (°C)	h[g] (km)	ϕ[g] (km/100)
Tonga																
Volcano 19	3.27	0.23	5.22	0.427	0.082	6,264	740	0.07	*730*	8,360		*730*				
Volcano 7	3.62	0.30	8.21	0.450	0.055	4,409	772	0.08	738	4,824		764				
Volcano A	4.66	0.17	2.24	0.100	0.045	20,804	*730*	0.04	*730*	21,400		*730*				
Tofua	4.16	0.15	5.35	0.211	0.039	7,776	*730*	0.04	*730*	7,742		*730*				
Volcano D	2.88	0.26	3.87	0.198	0.052	7,442	*730*	0.09	747	7,994		*730*				
Volcano F	2.43	0.27	3.91	0.218	0.056	6,215	741	0.11	768	6,873		732				
Volcano L	3.64	0.71	7.29	0.876	0.121	4,993	761	0.20	825	9,583		*730*				
Average	*3.52*	*0.30*	*5.16*	*0.354*	*0.064*	*8,272*	*744*	*0.09*	*752*	*9,539*		*735*	*733*	*733*	*123*	*143.2*
Marianas																
Sarigan	6.14	0.49	14.6	1.65	0.113	4,205	777	0.08	734	7,385		*730*				
Guguan	4.49	0.33	6.95	0.520	0.075	6,460	737	0.07	*730*	8,135		*730*				
Pagan	3.45	0.50	12.3	0.950	0.077	2,805	814	0.14	795	3,564		792				
Agrigan	5.40	0.25	17.5	1.19	0.068	3,086	805	0.05	*730*	3,675		789				
Average	*4.87*	*0.39*	*12.8*	*1.08*	*0.083*	*4,139*	*783*	*0.09*	*747*	*5,690*		*760*	*873*	*827*	*169*	*63.5*
Kamchatka																
Chikurachki	3.53	0.66	15.2	1.31	0.086	2,322	831	0.19	821		2,532	823				
Ksudach	3.55	0.16	6.41	0.515	0.080	5,538	752	0.05	*730*		5,994	744				
Karymsky	3.49	0.77	17.8	2.34	0.131	1,961	847	0.22	838		2,343	830				
Tolbachik	2.91	0.66	16.5	1.91	0.116	1,764	857	0.23	841		2,035	843				
Klyuchevskoy	7.09	0.57	14.7	1.30	0.088	4,823	764	0.08	735		5,305	755				
Average	*4.11*	*0.56*	*14.1*	*1.48*	*0.100*	*3,282*	*810*	*0.15*	*793*		*3,642*	*799*	*767*	*749*	*111*	*54.1*
Aleutians																
Korovin	4.48	0.92	26.3	3.24	0.123	1,703	860	0.21	830		1,994	845				
Seguam	3.43	0.27	7.76	0.829	0.107	4,420	772	0.08	733		5,052	760				
Okmok	3.34	0.61	16.6	2.98	0.180	2,012	844	0.18	818		2,689	818				
Pakushin (Unalaska)	3.54	2.43	17.9	1.75	0.098	1,978	846	0.69	954		2,203	836				
Akutan	3.66	0.38	14.8	1.38	0.093	2,473	826	0.10	761		2,736	816				
Shishaldin	2.37	1.08	31.8	6.17	0.194	745	936	0.46	912		979	911				
Emmons	2.68	1.01	25.0	4.08	0.163	1,072	902	0.38	892		1,348	881				
Augustine	6.70	0.44	16.2	1.10	0.068	4,136	778	0.07	*730*		4,362	773				
Average	*3.78*	*0.89*	*19.5*	*2.69*	*0.128*	*2,317*	*845*	*0.27*	*829*		*2,671*	*830*	*783*	*764*	*105*	*25.4*

Table 1. (continued)

	Arc Eruptives									Slab Fluids				Geophys. Thermal Models		
	H_2O[a] (wt%)	K_2O[a] (wt%)	Ce[a] (ppm)	Nb[a] (ppm)	Nb/Ce (ppm/ppm	H_2O/Ce (ppm/ppm)	Temp. (H_2O/Ce)[b] (°C)	K_2O/H_2O (wt%/wt%)	Temp. (K_2O/H_2O)[c] (°C)	H_2O/Ce; Projected From H-DMM[d] (ppm/ppm)	H_2O/Ce; Projected From E-MORB[d] (ppm/ppm)	Temp. (H_2O/Ce)[b] (°C)	Temp. (Corr.)[e] (°C)	Temp. (D80)[f] (°C)	h[g] (km)	ϕ[g] (km/100)
Cascadia																
Blue Lake	3.59	0.66	20.2	4.03	0.200	1,777	856	0.18	819		2,489	825				
Sand Mountain	2.56	0.96	46.5	10.1	0.217	551	963	0.38	892		736	937				
Garrison Butte	1.67	0.57	29.1	6.00	0.206	574	960	0.34	882		753	935				
Twin Craters	1.81	0.62	32.8	5.20	0.159	552	963	0.34	883		658	947				
Yapoah	3.01	0.65	23.3	4.80	0.206	1,292	885	0.22	836		1,814	854				
Island Fissure	2.66	0.92	45.6	14.0	0.307	583	958	0.35	884		999	909				
Collier	2.70	0.67	21.5	4.00	0.186	1,256	888	0.25	850		1,676	861				
Shasta	3.40	0.29	25.8	1.40	0.054	1,318	883	0.09	741		1,350	881				
Average	*2.68*	*0.67*	*30.6*	*6.19*	*0.192*	*988*	*919*	*0.27*	*848*		*1,309*	*894*	*809*	*888*	*90*	*1*
Mexico																
San Juan	2.90	0.84	28.8	10.9	0.378	1,007	908	0.29	866		2,572	822				
Astillero	4.00	0.59	16.7	3.30	0.198	2,395	828	0.15	797		3,369	797				
Hungaro	3.90	0.61	22.0	3.95	0.180	1,773	856	0.16	803		2,360	830				
Paricutin	4.90	0.75	23.2	4.76	0.205	2,112	840	0.15	800		3,020	807				
Jorullo	5.70	0.61	15.7	2.26	0.144	3,631	790	0.11	764		4,502	771				
Jumiltepec	3.00	1.25	55	5	0.091	545	964	0.42	903		584	958				
Las Tetillas	3.60	0.86	27	5	0.185	1,333	882	0.24	846		1,781	856				
Tuxtepec	5.20	1.72	113	2	0.018	460	980	0.33	879		449	982				
Tepetlapa	3.20	1.05	63	16	0.254	508	971	0.33	878		728	938				
Average	*4.04*	*0.92*	*40.5*	*5.91*	*0.184*	*1,529*	*891*	*0.24*	*837*		*2,152*	*862*	*752*	*780*	*80*	*4*
Guatemala																
Santa Maria	2.69	1.05	18.3	3.24	0.177	1,470	873	0.39	896		1,933	848				
Atitlan	3.10	1.37	29.5	5.02	0.170	1,051	904	0.44	909		1,340	882				
Fuego	3.76	1.34	24.0	4.03	0.168	1,567	867	0.36	887		2,021	844				
Agua	3.43	0.95	23.1	3.81	0.165	1,485	872	0.28	861		1,898	850				
Average	*3.25*	*1.18*	*23.7*	*4.03*	*0.170*	*1,393*	*879*	*0.37*	*888*		*1,798*	*856*	*901*	*885*	*142*	*9.7*
Nicaragua																
Cerro Negro	5.08	0.31	8.68	2.57	0.296	5,853	746	0.06	*730*		11,487	*730*				
Nejapa	1.86	0.10	6.88	2.14	0.311	2,703	817	0.05	*730*		5,508	752				
Granada	4.13	0.59	9.94	1.88	0.189	4,155	778	0.14	793		5,776	748				
Average	*3.69*	*0.33*	*8.50*	*2.20*	*0.265*	*4,237*	*781*	*0.09*	*751*		*7,590*	*743*	*856*	*878*	*169*	*11*

Table 1. (continued)

	Arc Eruptives									Slab Fluids				Geophys. Thermal Models		
	H_2O[a] (wt%)	K_2O[a] (wt%)	Ce[a] (ppm)	Nb[a] (ppm)	Nb/Ce (ppm/ppm	H_2O/Ce (ppm/ppm)	Temp. (H_2O/Ce)[b] (°C)	K_2O/H_2O (wt%/wt%)	Temp. (K_2O/H_2O)[c] (°C)	H_2O/Ce; Projected From H-DMM[d] (ppm/ppm)	H_2O/Ce; Projected From E-MORB[d] (ppm/ppm)	Temp. (H_2O/Ce)[b] (°C)	Temp. (Corr.)[e] (°C)	Temp. (D80)[f] (°C)	h[g] (km)	ϕ[g] (km/100)
Costa Rica																
Arenal	3.91	0.48	18.3	3.03	0.166	2,137	839	0.12	778		2,764	815	723			
Irazu	3.18	2.03	96.2	23.0	0.239	331	1010	0.64	946		413	990	897			
Average	*3.55*	*1.26*	*57.3*	*13.0*	*0.202*	*1,234*	*925*	*0.38*	*862*		*1,589*	*902*	*810*	*695*	*87*	*10.1*
Lesser Antilles																
St. Vincent	4.88	0.27	8.86	2.89	0.326	5,508	752	0.06	*730*		12,205	*730*	773	*838*	*141*	*10.4*

[a]Volatile, major element, and trace element compositions of arc eruptives for each volcano. H_2O and K_2O compositions from MIs. Ce and Nb from either WRs or MIs. See Text S1 for data treatment and sources.
[b]Fluid temperatures at 4 GPa, based on H_2O/Ce using equation (1) from *Plank et al.* [2009]. See section 2 for details. Temperatures lower than the wet solidus (730°C) were fixed to this temperature, as indicated by italics.
[c]Fluid temperatures at 4 GPa, based on K_2O/H_2O using the equation in section 4.2, which was originally published in the work of *Plank et al.* [2009] with an error. Temperatures lower than the wet solidus (730°C) were fixed to this temperature, as indicated by italics.
[d]Mantle-corrected H_2O/Ce compositions of slab fluids, estimated from a projection from the local mantle source through the arc eruptive to a Nb/Ce of 0.04. See section 3.2 for details. Local mantle source compositions for each subduction zone were inferred from *Plank* [2005], *Eiler et al.* [2005], *Johnson et al.* [2009], and *Ruscitto et al.* [2010]. We used an E-MORB local mantle source for the Nicaraguan and Lesser Antilles volcanoes (as opposed to N-MORB suggested by *Eiler et al.* [2005] and *Plank* [2005], respectively) because the volcanoes in these arcs have compositions similar to N-MORB, which leads to projections with a strong vertical (H_2O/Ce) trajectory.
[e]H_2O/Ce fluid temperatures adjusted to sub-arc slab surface depths, h, using equation (2). See section 3.3 for details.
[f]SASSTs, using the revised D80 thermal model of *Syracuse et al.* [2010]. See section 5.1 for details. The temperatures published in the work of *Syracuse et al.* [2010] incorporated a minor error in the temperature profile in the slab inflow boundary conditions, which led to slab temperatures for slabs older than 65 Ma that were erroneously less than 40°C colder than those used here. Subduction zone segments are the same, with the exception of the Marianas (S. Marianas), the Aleutians (E. Aleutians), Cascadia (C. Cascades), and the Lesser Antilles (S. Lesser Antilles).
[g]Subduction parameters, h (sub-arc depth to slab surface) and ϕ (thermal parameter), are from *Syracuse et al.* [2010].

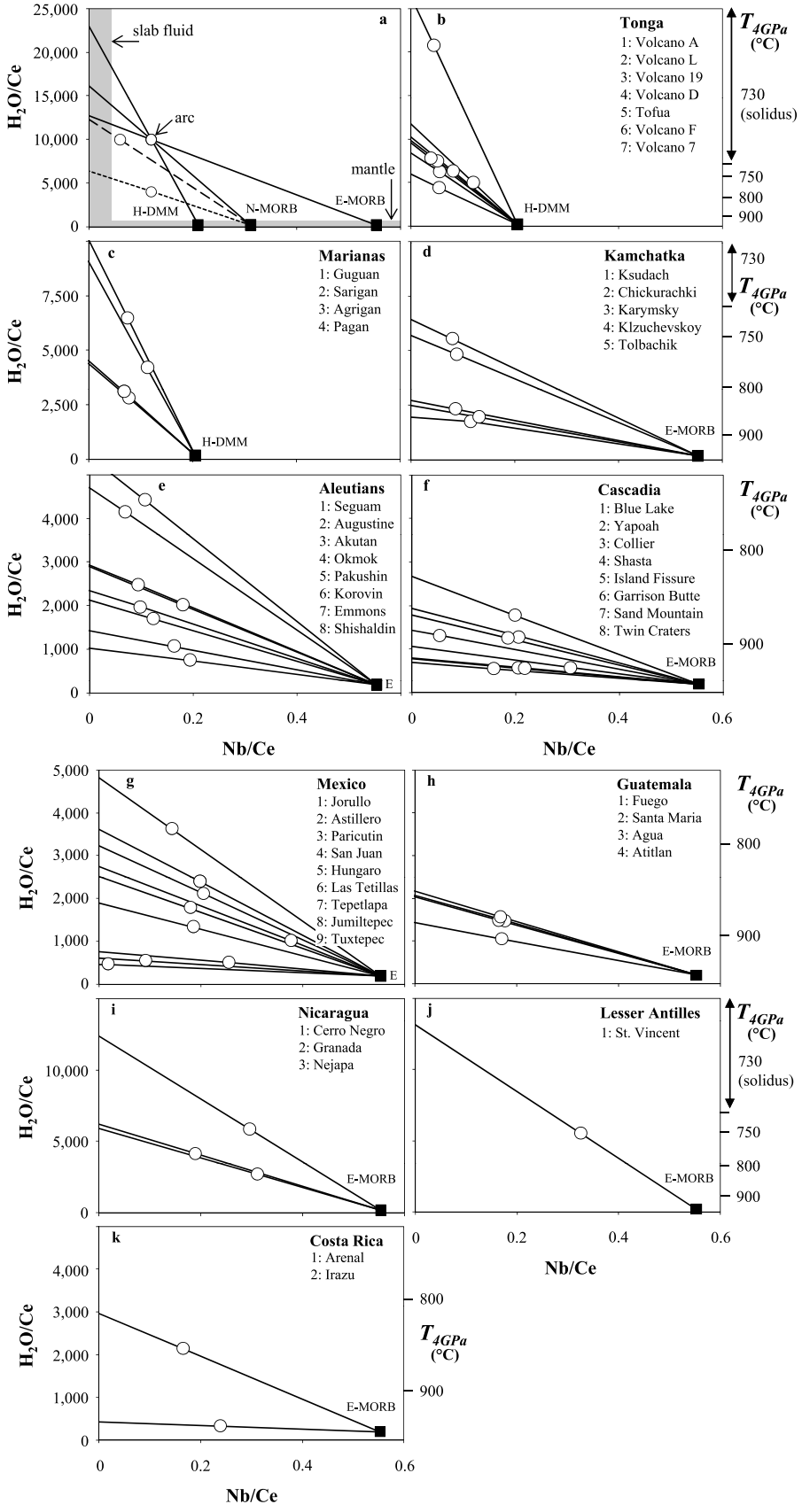
a
slab fluid
arc
mantle
H-DMM
N-MORB
E-MORB
b
Tonga
1: Volcano A
2: Volcano L
3: Volcano 19
4: Volcano D
5: Tofua
6: Volcano F
7: Volcano 7
c
Marianas
1: Guguan
2: Sarigan
3: Agrigan
4: Pagan
d
Kamchatka
1: Ksudach
2: Chickurachki
3: Karymsky
4: Klzuchevskoy
5: Tolbachik
e
Aleutians
1: Seguam
2: Augustine
3: Akutan
4: Okmok
5: Pakushin
6: Korovin
7: Emmons
8: Shishaldin
f
Cascadia
1: Blue Lake
2: Yapoah
3: Collier
4: Shasta
5: Island Fissure
6: Garrison Butte
7: Sand Mountain
8: Twin Craters
g
Mexico
1: Jorullo
2: Astillero
3: Paricutin
4: San Juan
5: Hungaro
6: Las Tetillas
7: Tepetlapa
8: Jumiltepec
9: Tuxtepec
h
Guatemala
1: Fuego
2: Santa Maria
3: Agua
4: Atitlan
i
Nicaragua
1: Cerro Negro
2: Granada
3: Nejapa
j
Lesser Antilles
1: St. Vincent
k
Costa Rica
1: Arenal
2: Irazu
H2O/Ce
Nb/Ce
T4GPa (°C)
730 (solidus)
750
800
900

Figure 5

Nb to Ce, and plot it against H_2O/Ce (Figure 5). This becomes a useful diagram for illustrating and quantifying the mixing process because: 1) Nb is incompatible like H_2O and Ce and so minimally fractionated during partial melting and crystallization; 2) mixing lines are linear due to common denominators; and 3) the mantle and slab fluid components are located near the Nb/Ce and H_2O/Ce axes, respectively, making mixing lines easy to interpret (i.e., the H_2O/Ce ratio of the mantle is very low compared to that of slab fluids, and the Nb/Ce of slab fluids are expected to be very low compared to that of different mantle sources). The Nb/Ce ratio is also a measure of the well-known "Nb-anomaly" common to arc magmas.

[21] For each volcano, the H_2O/Ce ratio of the slab fluid was estimated from a mixing line between the measured arc composition and an estimate of its mantle source (Figure 5). The slab fluid composition was calculated from the projection toward the *y* axis. In practice, we did not project all the way to the *y* axis (Nb/Ce = 0) because slab fluids will contain some Nb (i.e., finite Nb/Ce). We chose a Nb/Ce value of 0.04 for the slab fluid, as it was the minimum Nb/Ce value recorded in the arc compositions that we considered in this study (with the exception of Tuxtepec in Mexico), and therefore the maximum possible Nb/Ce for the slab fluids. Our assumption about Nb/Ce in the slab fluid leads to only a small shift in calculated temperatures (as can be deduced from Figure 5). Figure 5a shows the generic topology of the mixing problem. For a given arc composition, a highly depleted mantle source with low Nb/Ce (e.g., H-DMM) will lead to a projected slab fluid with higher H_2O/Ce than a more enriched mantle source with high Nb/Ce (e.g., E-MORB) (solid lines in Figure 5a). For a given mantle source composition and H_2O/Ce ratio in the arc, the arc with higher Nb/Ce will project to a slab fluid with higher H_2O/Ce than one with lower Nb/Ce (solid and long dashed lines, respectively, originating from N-MORB). Finally, for a given mantle source composition and Nb/Ce ratio in the arc, an arc eruptive with higher H_2O/Ce will project to a slab fluid with higher H_2O/Ce than one with lower H_2O/Ce (solid and short dashed lines, respectively, originating from N-MORB). Thus the geometry of the mixing problem depends critically on the relative positions of the arc and mantle source compositions, but in all cases, the slab fluid has higher H_2O/Ce than that measured in the arc eruptives, leading to a decrease in inferred slab fluid temperature compared to using the actual H_2O/Ce ratios measured in melt inclusions.

[22] The primary assumption in performing this correction is the Nb/Ce of the mantle. We chose a constant composition for each arc (guided by prior detailed studies on the geochemical variations in each arc; see Table 1 footnotes for references), even though within a single subduction zone, especially those with active backarc basins, mantle source compositions may be variable [*Cooper et al.*, 2010]. As is apparent from the examples given in Figure 5a, it is possible to generate a factor of 2 variation in H_2O/Ce from uncertainties in the mantle source (from enriched to depleted). A factor of 2 variation in slab fluid H_2O/Ce, however, leads to only a ~50°C variation in the predicted slab fluid temperature (at ~800°C), due to the logarithmic nature of the H_2O/Ce-temperature function. In section 4.2, we conclude that the magnitude of this mantle correction generally leads to an even smaller effect on the calculated temperatures (~20°C on average). Thus, the mantle is not generally a big contributor to arc H_2O/Ce, as we posited initially.

[23] The Nb/Ce-H_2O/Ce mixing diagram also illustrates how arc magmas with similar magmatic H_2O contents may originate from slab fluids with highly variable H_2O/Ce. For example, MIs from Tonga and Guatemala both have similar average least-degassed H_2O contents of (~3.25 to 3.5 wt%), and yet the H_2O/Ce of their slab fluids are completely

Figure 5. Determination of H_2O/Ce in slab fluid components by unmixing the mantle contribution from arc compositions. Figures show mixing lines for individual volcanoes between mantle source, arc eruptive, and slab fluid components on H_2O/Ce versus Nb/Ce plots. (a) Generic figure with slab fluid projections from three mantle source compositions (highly depleted MORB mantle [H-DMM], depleted MORB mantle [N-MORB], and enriched MORB mantle [E-MORB]) through three arc compositions (see section 3.2 for details). Shaded bands near the Nb/Ce and H_2O/Ce axes represent the expected compositional range for the mantle and slab fluids, respectively. (b–k) Slab fluid projections for individual volcanoes in each subduction zone from their preferred mantle sources (see references in Table 1 footnote). Within each arc, the ordering of the volcanoes (1, 2, 3, etc.) indicates decreasing H_2O/Ce of the slab fluid. Equivalent temperatures at 4 GPa are shown on the right *y* axis, calculated from the H_2O/Ce thermometer from *Plank et al.* [2009] given in equation (1). Note that the *y* axis scales are not consistent for all of the panels. Nb/Ce of H-DMM (0.205) from *Workman and Hart* [2005]; Nb/Ce of N-MORB (0.311) and E-MORB (0.553) from *Sun and McDonough* [1989]. H_2O/Ce of the mantle is 200 [*Michael*, 1995; *Dixon et al.*, 2002]. Nb/Ce of slab fluids is taken at 0.04 (see section 3.2 for details).

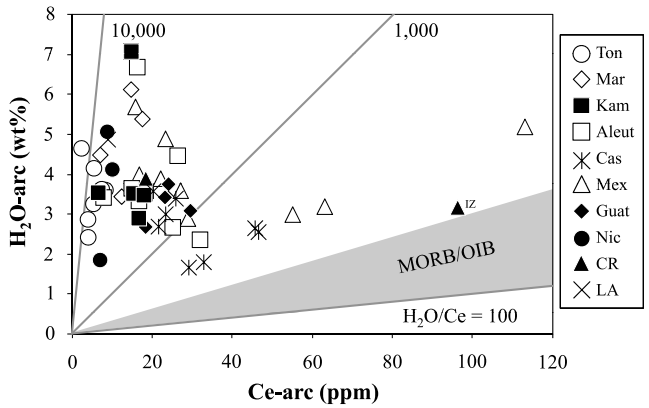

Figure 6. Variation in maximum (least-degassed) H_2O and Ce concentrations in arc eruptives for individual volcanoes from all of the subduction zones in this study. Different symbols denote different arcs, as labeled. MORB/OIB field is from *Michael* [1995] and *Dixon et al.* [2002].

dissimilar (~9,500 versus 1,800, respectively) (Table 1 and Figures 5b and 5h). While this is partly a function of mantle source composition (i.e., H-DMM versus in E-MORB, respectively) it results primarily from major inter-arc differences in the concentration of Ce in arc eruptives (e.g., ~5 ppm Ce for Tonga versus 25 ppm for Guatemala). On the other hand, some arc magmas have different H_2O while H_2O/Ce in their slab fluids is similar, such as Nejapa and Granada in Nicaragua (with nearly identical H_2O/Ce slab fluids compositions of ~5,600, but very different magmatic H_2O contents of 2 versus 4 wt%, respectively) (Figure 5i). In these cases, the relative H_2O concentration of an arc magma may be estimated from its position along the mantle source-slab fluid mixing line. Granada plots on the same line as Nejapa, but is closer to the slab fluid end-member, and therefore receives a larger relative fraction of the slab fluid and contains a higher magmatic H_2O content.

3.3. Pressure Correction of the H_2O/Ce Thermometer

[24] As described in section 2, the H_2O/Ce geothermometer is calibrated for pressures near 4 GPa. Temperatures at other pressures (see section 5 for the application to sub-arc slab surface depths) were estimated by projecting T_{4GPa} along H_2O-isopleths (in the supersolidus region), which are nominally linear and defined up to 4.5 GPa by *Hermann and Spandler* [2008] (Figure 4). By definition, the H_2O concentration in the melt is constant along each isopleth, and so this effect is explicitly taken into account in the pressure correction of H_2O/Ce temperatures. Because monazite solubility is likely dependent on solute content (100 - H_2O along the isopleth), Ce concentration may also be maintained in this projection. These are simplifying assumptions, with significant uncertainties on the shapes and slopes of the H_2O-isopleths, and further work will better guide how to translate H_2O/Ce through *P-T* space. Nonetheless, there is a better rationale for projecting H_2O/Ce along H_2O-isopleths than simply translating T_{4GPa} isothermally up or down pressure. Accordingly, we assume for the purpose of this work that isopleths of H_2O concentration have constant, linear slopes in the supersolidus and supercritical region. We propose the following parameterization (based on *Hermann and Spandler* [2008] and illustrated in Figure 4):

$$T_d = T_{4GPa} + 2.5 * (d - 124) \quad (2)$$

where d is the depth of interest (in km), 124 reflects depth (in km) at 4 GPa (assuming a mantle density of 3.3 g/cc), and 2.5 is the slope of the H_2O-isopleths (in °C/km).

4. Results

4.1. H_2O/Ce in Arc Magmas and Slab Fluids

[25] The H_2O/Ce ratios measured in arc magmas span nearly two orders of magnitude, from ~300 (Irazu volcano in Costa Rica) to 21,000 (Volcano A in Tonga; Table 1 and Figure 6). This is in stark contrast to the low values and narrow range of H_2O/Ce in the oceanic mantle (200 ± 100) [*Michael*, 1995; *Dixon et al.*, 2002]. The difference between the H_2O/Ce of arc and oceanic basalts is largely due to differences in H_2O content: while MORB have undegassed H_2O contents ≪ 1 wt% and OIB <

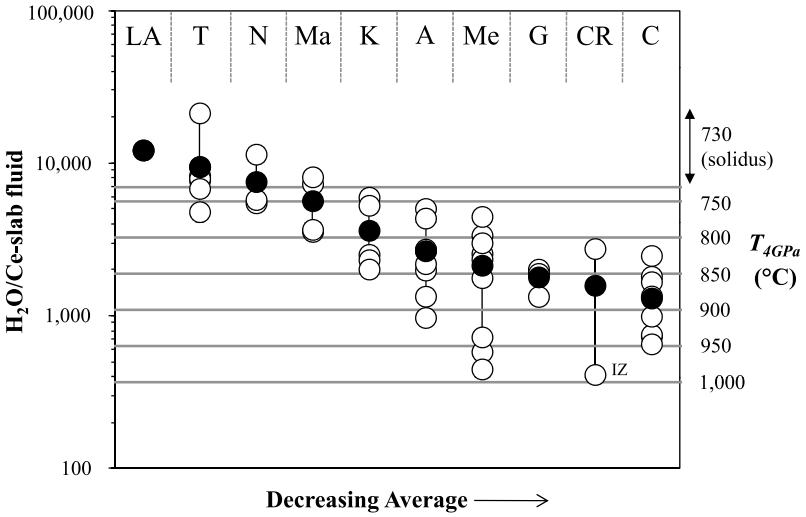

Figure 7. H_2O/Ce estimates of slab fluids after the mantle correction (as in Figure 5) for individual volcanoes grouped by arc. Vertical lines illustrate the entire range for each arc. The order of the volcanoes in each arc (from high H_2O/Ce to low H_2O/Ce) are consistent with the numbering scheme in Figure 5. Filled symbols represent the averages for each arc. Equivalent temperatures for 4 GPa, calculated from the H_2O/Ce thermometer from *Plank et al.* [2009] given in equation (1), are shown as horizontal lines in the plot corresponding to the right *y* axis.

2 wt% [*Michael*, 1995; *Dixon et al.*, 2002; *Workman et al.*, 2006], arc magmas have undegassed H_2O contents up to 7 wt% [*Wallace*, 2005; *Zimmer et al.*, 2010; *Auer et al.*, 2009]. The highest average H_2O/Ce ratios are in the Tonga, the Lesser Antilles, Nicaragua, and Mariana arcs (H_2O/Ce ~4,000 to 8,000); Kamchatka and the Aleutians have intermediate ratios (~2,000 to 3,000); and Mexico, Guatemala, Costa Rica, and Cascadia have the lowest ratios (~1,000 to 1,500). The large range in H_2O/Ce is due to variations in both H_2O and Ce — while Ce varies more than H_2O (factor of 50), the H_2O variations are significant as well (factor of 4; Figure 6).

[26] As discussed earlier, subtracting the mantle contribution to H_2O/Ce raises this ratio in the inferred slab fluid, regardless of which mantle source composition is assumed. Taking into account the best constraints available on the appropriate mantle source for each arc (see references in Table 1 footnotes) leads to a range in H_2O/Ce in the slab fluid from ~400 to 21,000, nearly the same as in the arc eruptives themselves (Table 1 and Figure 7). The relative differences between the arcs also remain the same. The largest correction involves a factor of ~2.5 increase in H_2O/Ce for San Juan volcano in Mexico, due to its relatively high measured Nb/Ce. For some of the volcanoes, the correction depends critically on the composition of the enriched mantle (Figure 5), which is generally not well known, and so the estimates of slab fluid temperature for these volcanoes are highly uncertain.

[27] We obtain a wide range in H_2O/Ce in global slab fluids (Figure 7). This agrees with prior estimates in the literature, which are typically based on inverting trace element and isotopic compositions to solve for mantle melting, mixing and source (Figure 8). For example, estimated slab fluids beneath the Mariana and Lau back-arc basins have H_2O/Ce of ~2,000 and 10,000, respectively [*Stolper and Newman*, 1994; *Bézos et al.*, 2009]. Slab fluids calculated with MIs from Kamchatka, Cascadia and Mexico yield H_2O/Ce of ~2,000 to 3,000 [*Grove et al.*, 2002; *Cervantes and Wallace*, 2003; *Portnyagin et al.*, 2007; *Johnson et al.*, 2009; *Ruscitto et al.*, 2010]. Other experimental [*McDade et al.*, 2003] and oxygen isotopic studies [*Eiler et al.*, 2000; *Eiler et al.*, 2005] have proposed H_2O/Ce of ~2,000 to 7,000 in different slab fluids, although these studies lacked actual H_2O measurements to guide their estimates. As with prior estimates, our unmixing approach yields greater magnitudes and a wider range of H_2O/Ce in slab fluids than are found in MORB or OIB (Figure 8).

4.2. Apparent Slab Fluid Temperatures at 4 GPa

[28] Apparent slab fluid temperatures of individual volcanoes at 4 GPa can be calculated from H_2O/Ce

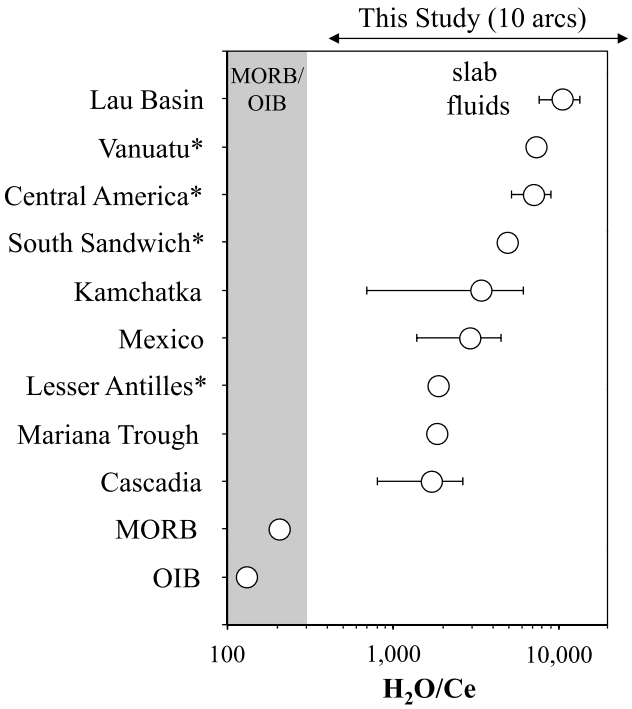

Figure 8. Published estimates of the H_2O/Ce ratio for MORB, OIB, and slab fluids. Symbols with error bars represent averages ± 1 standard deviation. MORB/OIB field from *Michael* [1995] and *Dixon et al.* [2002]. MORB from Discovery, Shonas, and FAZAR [*Dixon et al.*, 2002] and Easter Microplate [*Simons et al.*, 2002]. OIB from Samoa [*Workman et al.*, 2006], Loihi [*Dixon and Clague*, 2001], and Easter/Salas y Gomez [*Simons et al.*, 2002]. Estimates for Cascadia from *Grove et al.* [2002] and *Ruscitto et al.* [2010]; the Mariana Trough from *Stolper and Newman* [1994]; the Lesser Antilles and South Sandwich arcs from *McDade et al.* [2003]; Mexico from *Cervantes and Wallace* [2003] and *Johnson et al.* [2009]; Kamchatka from *Portnyagin et al.* [2007]; Central America from *Eiler et al.* [2005]; Vanuatu from *Eiler et al.* [2000]; and the Lau Basin from *Bézos et al.* [2009]. Estimates with * involved no actual measurements of H_2O.

ratios using the thermometer given in equation (1) [*Plank et al.*, 2009]. Correcting for local mantle source compositions has a small effect on estimated slab fluid temperatures of individual volcanoes, lowering temperatures by ∼20°C on average. This shift is well within the uncertainty of the fluid thermometer (at least 50°C; Figure 3). In light of these results, users should generally be confident in calculating temperatures from H_2O/Ce measured in arc melt inclusions alone, without the extra step of removing the mantle contribution. However, in this paper we report the mantle-corrected slab fluid temperatures. In the following section, these temperatures will be adjusted to sub-arc depths to estimate average sub-arc slab surface temperatures for each arc.

[29] Slab fluid temperatures at 4 GPa for individual volcanoes range globally from 730°C to 990°C (Table 1 and Figure 7). In detail, the average slab fluid T_{4GPa} is < 750°C for the Lesser Antilles, Tonga, and Nicaragua; between ∼750 and 800°C for the Marianas and Kamchatka; between ∼800 and 850°C for the Aleutians and Guatemala; and between ∼850 and 900°C for Mexico, Cascadia and Costa Rica.

[30] The calculated apparent temperatures at 4 GPa are consistent with those determined using other geochemical approaches, specifically for Kamchatka (700 to 900°C at 4 GPa [*Portnyagin et al.*, 2007]) and Tonga (∼800°C at 2.5 GPa [*George et al.*, 2005]). The H_2O/Ce temperatures are also consistent with the independent K_2O/H_2O fluid thermometer proposed by *Hermann and Spandler* [2008] and parameterized by *Plank et al.* [2009] (note publisher's typo in their Figure 2b: the expression should be $K_2O/H_2O = 6 \times 10^{-5}\ e^{0.0098*T}$). As mentioned above, the K_2O/H_2O fluid thermometer is based on the solubility of phengite, which may have a very broad stability field on both sides of the solidus for K-rich, sedimentary compositions [*Schmidt et al.*, 2004; *Hermann and Spandler*, 2008; *Hacker*, 2008]. Fluid saturated with phengite

will increase in K_2O/H_2O by over an order of magnitude, from < 0.1 to > 1, as temperature increases from ~700 to 1,050°C at 3.5 to 4.5 GPa [*Hermann and Spandler*, 2008]. In Table 1, we compare slab fluid temperatures estimated from both the H_2O/Ce and K_2O/H_2O fluid thermometers (both at 4 GPa), using arc eruptive compositions. We find that the slab fluid temperatures for most of the individual volcanoes agree within 50°C, although some differ by > 100°C. The average arc temperatures, however, which are the focus of our discussion, agree within 35°C on average, although the K_2O/H_2O temperatures are systematically shifted to lower values than the H_2O/Ce temperatures for all arcs except Tonga and Guatemala. The general agreement in the relative and absolute slab fluid temperatures estimated from both thermometers is encouraging, given all the independent uncertainties that go into them.

5. Discussion

5.1. Sub-arc Slab Surface Temperatures

[31] One of the major goals of this study was to test whether the H_2O/Ce geothermometer yields temperatures that agree with those predicted from numerical models describing the thermal structure of subducting slabs. A relevant point of comparison is sub-arc slab surface temperature (SASST) — the temperature of the slab surface directly beneath the arc, at a depth of h — as this describes the region where fluids that supply the arc may have last equilibrated with the slab. Of course, this assumption could be incorrect, as fluids may also move laterally into the arc melting region, and so reflect shallower conditions than h [*Cagnioncle et al.*, 2007], or they may move updip from depths greater than h to reach the arc melting region [*Spiegelman et al.*, 2008]. Regardless, our starting assumption is that slab fluids equilibrate at the slab surface and flow predominantly vertically, such that the H_2O/Ce ratio in magmas reflects the conditions directly beneath the arc.

[32] In order to estimate SASST, arc-averaged mantle-corrected H_2O/Ce temperatures at 4 GPa were adjusted for h, which varies here from 80 km (Mexico) to 169 km (Nicaragua and the Marianas) (*Syracuse et al.* [2010]; see section 3.3 for details concerning the depth correction). We compare our H_2O/Ce results (Table 1 and Figure 2) to the SASSTs predicted from the thermal models of *Syracuse et al.* [2010]. We use the *Syracuse et al.* [2010] study in large part because they include all of the subduction zones we have examined. In their approach, parameters for each arc sector (i.e., geometry, convergence rate, plate age, sediment thickness and upper plate structure) are input into a two-dimensional kinematic model [from *van Keken et al.*, 2002] that is used to predict the thermal structure of the slab and mantle wedge as they interact. The wedge has a non-Newtonian, temperature- and stress-dependent rheology, with an initial potential temperature of 1420°C. The model does not include the effects of viscous dissipation, adiabatic heating or cooling, shear heating on the slab surface, mantle melting, or secondary convection in the wedge. *Syracuse et al.* [2010] do, however, examine the effect of slab-mantle coupling depth, which controls how and where the slab heats. At depths shallower than 50 km, the slab and wedge are assumed to be completely decoupled (full slip) and the slab heats slowly; at greater depths, the slab and wedge are assumed to be completely viscously coupled (no slip) and the slab heats rapidly; there is a transition region where the wedge moves at 5% of the plate rate. The SASST depends to some degree on the coupling depth. We choose the "D80" model from *Syracuse et al.* [2010], which assumes a constant coupling depth of 80 km for all slabs, to be representative as it is simple to interpret. For the 10 arcs considered here, the D80 model produces SASSTs within ~15°C on average of their "X25" model (coupling depth 25 km trenchward of the arc) and within ~40°C of their "W1300" model (coupling depth resulting in a maximum temperature of 1300°C beneath the arc). As *Syracuse et al.* [2010] note, the agreement with the fourth model, "T550," (coupling depth where the slab surface is 550°C) is similar for some arcs, but wildly different for others (such as Tonga). We do not consider the X25, W1300, or T550 models here.

[33] Figure 9 compares the SASSTs derived from H_2O/Ce to those predicted from the D80 model. There is a strong correlation between the SASSTs (r = 0.81, for all arcs with three or more volcanoes). The temperatures agree within 80°C and the average agreement is ~30°C. The large difference for Cascadia (~79°C) may be related to its weakly defined seismic zone, which causes uncertainty in slab geometry and h. When Cascadia is excluded, the average agreement in SASSTs is ~20°C and the regression improves (r = 0.92). Moreover, h for Cascadia (90 km) is very near the assumed coupling boundary (80 km), where temperatures change rapidly; moving h down or the coupling depth up by as little as 10 km would reconcile the temperature off-set. Although not included in the

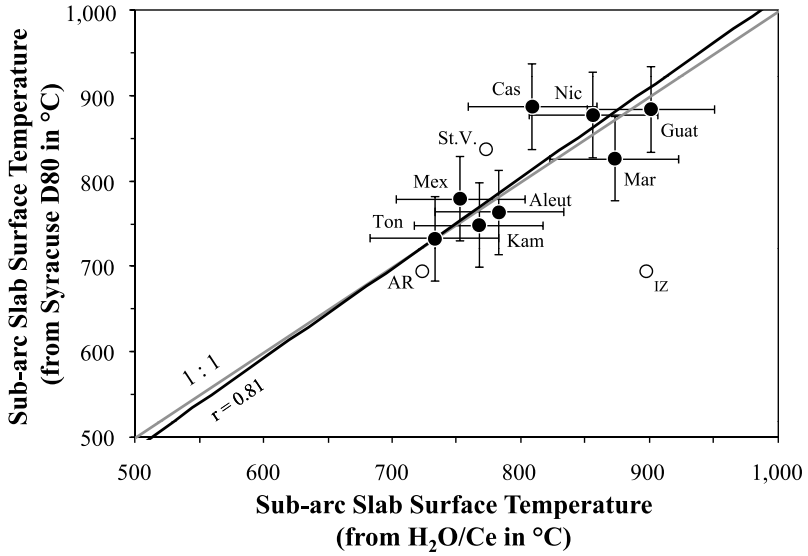

Figure 9. Comparison of SASSTs from H_2O/Ce measurements in arc magmas (this study) and the subduction thermal model of *Syracuse et al.* [2010]. H_2O/Ce SASSTs were calculated from arc melt compositions corrected for mantle contributions (i.e., slab fluids, as in Figure 5) using the thermometer in the work of *Plank et al.* [2009] given in equation (1), and then adjusted to reflect the pressure (depth) under each arc (h) using equation (2) (see section 3.3 and Figure 4 for details). Temperatures along the y axis are from the D80 model in the work of *Syracuse et al.* [2010] at h (see Table 1 footnotes for details). A reduced major axis regression (black line) from *Till* [1974] includes only arcs with three or more volcanoes (filled circles). The variable r is the Pearson correlation coefficient. The volcanoes not included in the regression are Arenal and Irazu in Costa Rica and St. Vincent in the Lesser Antilles (open circles). The 1:1 line (gray line) is shown for reference. Error bars for both axes are ± 50°C, which are minima.

regression, Irazu has either an anomalously high H_2O/Ce SASST or an anomalously low D80 SASST (see section 5.3 for possible explanations). Overall, Figure 9 indicates remarkable agreement between the two independent approaches, given the uncertainties in the thermometer (H_2O-isopleth contours, compositional effects on monazite solubility), the thermal models (mantle temperature, shear heating, coupling depth), and h (location of seismicity). The correlation also supports a nominally vertical transport path of slab fluids from their release at sub-arc depths toward the surface, and precludes crustal processes as the driver of global variations in H_2O/Ce temperatures.

[34] Both the geochemical and geophysical approaches for recovering SASST share important systematics. Slab surface temperatures at shallow depths (~30 km) or depths significantly greater than the coupling depth (here assumed to be 80 km), are reasonably well approximated by the thermal parameter, the product of slab age and vertical descent rate [*Syracuse et al.*, 2010, Figure 12]. Old slabs that descend rapidly (such as Tonga) have a high thermal parameter and are cooler at a given depth than young slabs that descend slowly (such as Cascadia) (Table 1). This is the primary reason that the D80 model predicts SASSTs for these two arcs to be ~150°C different, and indeed, they are end-member arcs in terms of H_2O/Ce SASST. On the other hand, for any given slab P-T path, temperature increases with depth, and so the depth of the sub-arc slab surface is also important. This effect can be seen when comparing Guatemala to Cascadia. On the basis of its thermal parameter alone, the Guatemala slab should be ~170°C cooler than the Cascadia slab at any given depth (estimated from the difference in D80 slab surface temperatures at 30 and 240 km), however, because sub-arc depths in Guatemala (h = 142 km) are much greater than Cascadia (h = 90 km), they both yield similar SASSTs from the D80 model. It is noteworthy that the H_2O/Ce thermometer also predicts the highest SASST for Guatemala, mostly due to its deep sub-arc slab depth. This effect is also observed between Mexico and the Marianas, where the very low thermal parameter for Mexico is offset by its shallow sub-arc slab depth (h = 80), producing a SASST warmer than the Marianas (h = 169 km). Thus, there is a surprisingly simple theory related to the thermal parameter that describes the thermal structure of slabs beneath arcs [*Syracuse et al.*, 2010; *van Keken et al.*, 2011], and this theory, combined with observed variations in h, is supported by the strong

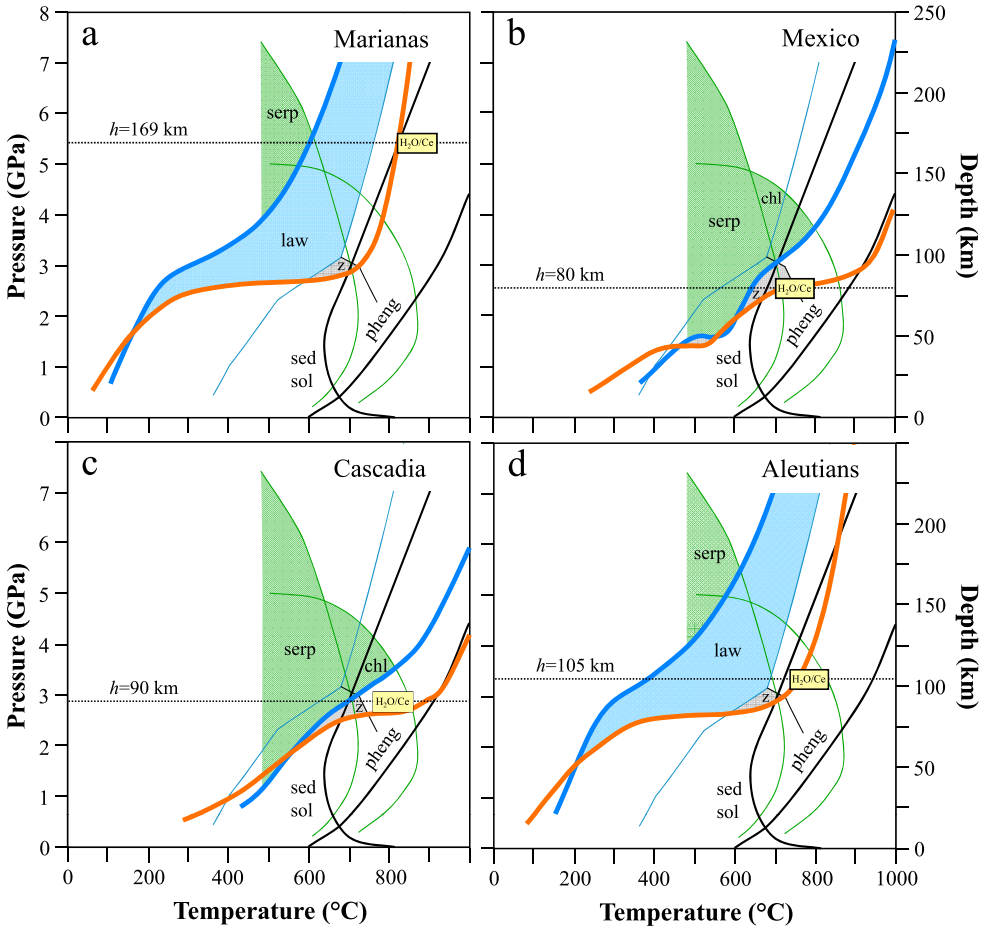

Figure 10. Slab thermal structure, key dehydration reactions, and H_2O/Ce temperatures for four subduction zones: (a) the Marianas, (b) Mexico, (c) Cascadia, and (d) the Aleutians. Subducting plate *P-T* paths, in orange (slab surface) and blue (slab Moho), are from the D80 model in the work of *Syracuse et al.* [2010] (see Table 1 footnotes for details). Yellow box represents the slab fluid temperatures (±50°C) of the respective arcs calculated from the H_2O/Ce thermometer of *Plank et al.* [2009] given in equation (1) (from Table 1), and adjusted to *h* [from *Syracuse et al.*, 2010]. Water-saturated sediment solidus and fluid-absent phengite melting curves (in black) after *Hermann and Spandler* [2008]. Blue, gray, and green shaded regions are where lawsonite and zoisite are stable in the subducting oceanic crust, and serpentine and chlorite are stable in the slab sub-Moho mantle based on phase boundaries in the work of *Schmidt and Poli* [1998].

agreement in the H_2O/Ce slab fluid temperatures recorded in arc magmas.

[35] While there is strong agreement between the H_2O/Ce temperatures and the thermal models from *Syracuse et al.* [2010], which are based on the original work of *van Keken et al.*, [2002], other thermal models predict slab temperatures too low to be consistent with the order of magnitude variation we observe in the H_2O/Ce ratios. Model results from *England and Wilkins* [2004] and *Iwamori* [2007] differ significantly from those of *Syracuse et al.* [2010], likely because they do not include a temperature-dependent mantle wedge rheology nor as high of a mantle potential temperature (1300 versus 1420°C). Other models include weak and buoyant materials that become unstable and flow or convect upward [*Gerya et al.*, 2002; *Gerya and Stoeckhert*, 2006] (Figure 1a), cooling the forearc and wedge to a large degree [*Castro and Gerya*, 2008]. While such instabilities may develop, H_2O/Ce limits the extent to which they can dominate flow with cool upwellings. Models that include a large low viscosity channel along the slab [*Iwamori*, 2007; *Hebert et al.*, 2009] (Figure 1b) lead to decoupling of the induced corner flow in the mantle that heats the slab. Although there is independent geophysical evidence for low viscosity regions in the mantle wedge [*Hebert and Gurnis*, 2010], H_2O/Ce again limits the extent to which it can perturb

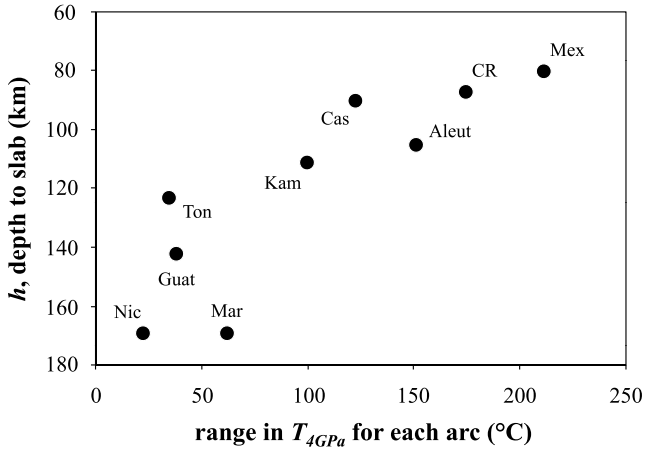

Figure 11. Relationship between the full range of temperatures calculated from H_2O/Ce for each arc at 4 GPa versus *h* [from *Syracuse et al.*, 2010].

flow and inhibit slab heating. The robust constraint from H_2O/Ce is that every arc we have examined shows evidence for slab surface temperatures on or above the H_2O-saturated sediment solidus (≥ 730°C at 3.5 to 4.5 GPa), and if these other thermal models (that predict uniformly lower temperatures) were correct, H_2O/Ce should be an order of magnitude higher than observed, reflecting conditions within the sub-solidus region.

5.2. Implications for *h*, Depth to the Slab Beneath the Arc

[36] This study provides constraints not just on SASST, but also on the kinds of reactions that may release fluids, drive melting in the mantle wedge, and potentially control the locus of volcanism at the surface. The 10 arcs considered here span a large range in *h*, from 80 to 169 km. Our first order result is that volcanoes clearly do not form in response to a critical isotherm in the slab, as both the numerical models and H_2O/Ce predict large variations in SASST between the arcs, from ∼730°C beneath Tonga to 900°C beneath Guatemala (Table 1 and Figure 2). Instead, temperatures range from the H_2O-saturated sediment solidus to ∼200°C above it. We can also conclude from this that arcs do not form as soon as slab *P-T* paths cross the H_2O-saturated sediment solidus. In many cases, arcs form when slabs have already passed this point (e.g., the Marianas; Figure 10a), and so while sediment melting is ubiquitous, it does not appear to be the limiting control on volcano position.

[37] Another prediction of the thermal models is that arcs with shallow *h*, within the slab-wedge coupling transition (generally observed between 60 and 80 km [*Wada and Wang*, 2009; *Syracuse et al.*, 2010]), might erupt a greater diversity of magma compositions, due to the wide range of slab surface temperatures that exist at this transitional depth. Figure 11 plots *h* versus the total range of H_2O/Ce-based slab fluid temperatures at 4 GPa for individual volcanoes from each arc. As we do not expect *h* to vary greatly within a given arc, these temperature ranges should also apply to SASSTs. We find a clear trend, where arcs that overlie shallow *h* slabs (∼80 to 100 km) sample a large range of inferred slab fluid temperatures, up to ∼200°C, in a region defining a significant portion of sediment melting between the wet solidus and phengite-out (Figures 10b, 10c, and 10d). This observation is consistent with the wide variety of magma types found in Cascadia (OIB, low-K olivine tholeiite, calc-alkaline basalt, high-magnesian andesite). The works by *Reiners et al.* [2000] and *Rowe et al.* [2009] attribute geochemical variability in Cascadia to differences in the *amount* of slab derived component, but the variability could also derive in part from the predicted variability in slab fluid *temperature*. Similarly, eruptives from Mexico (OIB, calc-alkaline basalt and basaltic andesite, shoshonite) and Costa Rica (shoshonite at Irazu and low-K basaltic andesite and andesite at Arenal) are quite diverse. Arcs with large *h* (>120 km) erupt more homogeneous magmas in terms of H_2O/Ce, with <∼50°C difference in inferred slab fluid temperatures, consistent with the nearly isothermal shape of the slab *P-T* paths in this region (Figure 10a). Thus, there is evidence that arcs that sample the shallow portion of the subduction zone

sample slab fluids with a wide range of formation temperatures, derived from the thermal "ledge" that forms as the mantle becomes viscously coupled to the slab, while arcs that sample slabs at greater depths have more homogenous chemistry reflecting a more thermally homogeneous slab surface. An alternate explanation is that beneath the arcs with large h, fluids have a longer vertical path through the mantle to follow, which might lead to homogenization by fluid mixing or reactions in the mantle.

5.3. Implications for Dehydration and Melting Reactions

[38] Slab fluid temperatures calculated with the new H_2O/Ce fluid thermometer are consistent with or greater than the H_2O-saturated solidus for both MORB and sediment (both 700°C < T_{sol} < 750°C at 3 GPa [*Schmidt et al.*, 2004; *Hermann and Spandler*, 2008; *Skora and Blundy*, 2010a; *Mibe et al.*, 2011]) for all subduction zones considered here (Table 1 and Figure 2). As such, the "fluid" that is liberated from the slab and migrates into the mantle wedge at sub-arc depths is likely to be a hydrous melt or a solute-rich supercritical fluid. There is no evidence for dilute, sub-solidus, aqueous fluids directly supplying the arc, because this would require arc magmas to have much higher H_2O/Ce (>100,000) than they do. However, at solidus temperatures, melts may have elevated H_2O contents verging toward that of aqueous fluids [*Ruscitto et al.*, 2012, Figure 10b]. This overall observation requires substantial revision of the commonly envisioned H_2O-rich, aqueous slab fluids that permeate the subduction zone literature. Instead, our H_2O/Ce results indicate that slab components likely contain <30 wt% H_2O [*Plank et al.*, 2009], and may have very different transport properties, compositions and viscosities than aqueous fluids.

[39] Although this study provides strong evidence for melting at the slab surface, this does not mean that aqueous fluid production isn't critical for the melting process itself. There are several ways to melt slab sediment, involving external and internal H_2O. If no H_2O is supplied to the sediment layer, the internal H_2O, predominantly hosted in the mica mineral phengite [*Hacker*, 2008], will drive melting at the fluid-absent phengite-dehydration solidus. This occurs at fairly high temperatures (>950°C at >100 km [*Hermann and Spandler*, 2008; *Schmidt et al.*, 2004]), higher than typically reached by most slabs. The exceptions are the slabs with low thermal parameter (like in Mexico and Cascadia), where young oceanic crust subducts and heats along high T/P trajectories that may intersect the phengite-out boundary (Figures 10b and 10c). Indeed, only in these arcs do volcanoes record H_2O/Ce temperatures that approach the phengite-out curve (with T_{4GPa} ~950°C for Tuxtepec, Jumiltepec and Tepetlapa in Mexico; and Twin Craters, Sand Mountain, and Garrison Butte in Cascadia). These arcs also lie near the fluid-absent amphibole-dehydration solidus in basalt [*Vielzeuf and Schmidt*, 2001], potentially implicating amphibole as another source of internal H_2O. Irazu volcano, at the end of the Costa Rica arc, is a conundrum in this respect. It records the lowest H_2O/Ce and therefore the highest T_{4GPa} of any arc volcano, and yet overlies a slab not predicted to ever cross the phengite-out curve. It is possible that either the thermal models underpredict temperatures at slab edges, which require three-dimensional treatments [*Kneller and van Keken*, 2008]; or that the H_2O/Ce thermometer is overpredicting temperatures at Irazu due to the subduction of a large section of Galapagos-derived volcaniclastics [*Benjamin et al.,* 2007], with atypical major element concentrations (i.e., altered alkali basalt), which may promote higher REE concentration in monazite/allanite-saturated melts than those used to calibrate the H_2O/Ce thermometer. Such enhancement of allanite/monazite solubility would be consistent with observations of crustal metamorphism and is supported by elevated F in Irazu magmas (up to 2,500 ppm [*Pan and Fleet*, 1996; *Benjamin et al.*, 2007]). Nonetheless, sediment melting at the fluid-absent, phengite-out boundary is likely rare, and limited to the hottest slabs.

[40] Based on their H_2O/Ce ratios, most volcanoes reflect sediment melting in the fluid-present melting region within ~150°C of the H_2O-saturated solidus at 4 GPa, and therefore require addition of external H_2O (Figure 1a). Likely sources derive from the dehydration reactions that occur below the sediment, in the cooler portions of the plate, where oceanic crust undergoes blueschist to eclogite reactions and mantle serpentinized peridotite dehydrates [*Hacker*, 2008]. Major H_2O-liberating reactions involve lawsonite breakdown in the basaltic oceanic crust and serpentine breakdown in the sub-slab Moho peridotite (provided these deeper regions of the downgoing plate are indeed hydrated prior to subduction). The thermal structures of different slabs point to different reactions that may supply some arcs versus others. For example, the Mariana

arc overlies great enough slab depths (~170 km) that serpentine and lawsonite are likely to be major sources of H_2O for driving sediment melting at the slab surface (Figure 10a). Moreover, at these depths, the slab surface barely nicks the H_2O-saturated solidus, and so it is unlikely that the colder, hydrous oceanic crust below will melt also. This is consistent with the highly systematic geochemical variations in the Mariana volcanoes, which have been interpreted to reflect mixing of two components from the slab, one an aqueous fluid from the MORB crust and the other a sediment melt [*Elliott et al.*, 1997]. This contrasts with other arcs, such as Cascadia, (Figure 10c), where a very large proportion of the oceanic crust exists above its wet solidus [*van Keken et al.*, 2011]; in this case, basaltic melts of the slab may outweigh sediment melts and adakites could be generated [*Defant and Drummond*, 1990]. The Mount Shasta region of the Cascades does contain high Mg# andesites with somewhat elevated $\delta^{18}O$ and Sr/Y [*Grove et al.*, 2002; *Martin et al.*, 2011, *Ruscitto et al.*, 2011] (note though that the elevated $\delta^{18}O$ is argued to be from much older mantle enrichment), but primitive and near-primitive magmas in most other regions of the Cascades are primarily basalts with normal $\delta^{18}O$ and Sr/Y [*Ruscitto et al.*, 2010], which seems inconsistent with basalt melting in the slab. While we have focused on the slab surface temperature, envisioning final equilibration of fluids there, fluids from greater depth in the slab will still have the ability to transport elements that reflect their lower temperature origin (e.g., Ba, Pb, Sr), and so contribute to the final composition of the composite fluid leaving the slab.

6. Conclusions

[41] In this paper, we have applied the H_2O/Ce thermometer of *Plank et al.* [2009] to arc compositions to estimate slab fluid temperatures at sub-arc slab depths for 51 volcanoes in 10 subduction zones. In doing so, we developed a new projection for slab fluid temperatures to pressures and depths beyond the original 4 GPa calibration, and also incorporated a new mantle correction scheme. Our results agree remarkably well on an arc-to-arc basis with sub-arc slab surface temperatures generated by thermal models from *Syracuse et al.* [2010]. Together, the volcanic data and thermal models demonstrate that global variations in slab fluid temperature and magma composition may be related to the slab thermal parameter and depth beneath the arc in a straightforward way. The calculated temperatures are all on or above the wet-sediment and wet-basalt solidi, indicating that hydrous slab and sediment-derived melts and/or solute-rich supercritical fluids supply the arc melting regime in the mantle wedge, not aqueous fluids.

[42] The agreement between the H_2O/Ce thermometer and the thermal models is an achievement toward reconciling geochemical and geophysical observations. Historically, studies in both domains have been geared toward specific volcanoes or subduction zones in general. While this approach has been useful for gaining insight into a particular locality or an overview of subduction processes, new efforts have provided regional data with a global view. The convergence of data and model in predicting slab thermal structures provides new confidence in attacking the next part of the path–mantle wedge flow and melt transport.

Acknowledgments

[43] We wish to thank Susanne Skora and Michael Rowe for their constructive reviews of the manuscript. Thanks to Peter van Keken and Brad Hacker for useful discussions and to Jeremy Zechar for statistical advice. This work was supported by the U.S. National Science Foundation grants OCE-0839061 and OCE-0526450 (TP and LBC), and the Swiss National Science Foundation grant 20_125019 (LBC).

References

Anderson, A. T. (1979), Water in some hypersthenic magmas, *J. Geol.*, *87*, 509–531, doi:10.1086/628443.

Antignano, A., and C. E. Manning (2008), Rutile solubility in H_2O, H_2O–SiO_2, and H_2O–$NaAlSi_3O_8$ Fluids at 0.7–2.0 GPa and 700–1000°C: Implications for mobility of nominally insoluble elements, *Chem. Geol.*, *255*, 283–293, doi:10.1016/j.chemgeo.2008.07.001.

Arcay, D., E. Tric, and M.-P. Doin (2007), Slab surface temperature in subduction zones: Influence of the interplate decoupling depth and upper plate thinning processes, *Earth Planet. Sci. Lett.*, *255*, 324–338, doi:10.1016/j.epsl.2006.12.027.

Auer, S., I. Bindeman, P. Wallace, V. Ponomareva, and M. Portnyagin (2009), The origin of hydrous, high-d^{18}O voluminous volcanism: Diverse oxygen isotope values and high magmatic water contents within the volcanic record of Klyuchevskoy volcano, Kamchatka, Russia, *Contrib. Mineral. Petrol.*, *157*, 209–230, doi:10.1007/s00410-008-0330-0.

Benjamin, E. R., T. Plank, J. A. Wade, K. A. Kelley, E. H. Hauri, and G. E. Alvarado (2007), High water contents in basaltic magmas from Irazú Volcano, Costa Rica, *J. Volcanol. Geotherm. Res.*, *168*, 68–92, doi:10.1016/j.jvolgeores.2007.08.008.

Bézos, A., S. Escrig, C. H. Langmuir, P. J. Michael, and P. D. Asimow (2009), Origins of chemical diversity of back-arc basin basalts: A segment-scale study of the Eastern

Lau Spreading Center, *J. Geophys. Res.*, *114*, B06212, doi:10.1029/2008JB005924.

Brenan, J., H. Shaw, F. Ryerson, and D. Phinney (1995), Mineral-aqueous fluid partitioning of trace elements at 900°C and 2.0 GPa: Constraints on the trace element chemistry of mantle and deep crustal fluids, *Geochim. Cosmochim. Acta*, *59*, 3331–3350, doi:10.1016/0016-7037(95)00215-L.

Cagnioncle, A.-M., et al. (2007), The effect of solid flow above a subducting slab on the water distribution and melting at convergent plate boundaries, *J. Geophys. Res.*, *112*, B09402, doi:10.1029/2007JB004934.

Castro, A., and T. V. Gerya (2008), Magmatic implications of mantle wedge plumes: Experimental study, *Lithos*, *103*, 138–148, doi:10.1016/j.lithos.2007.09.012.

Caulfield, J. T., S. P. Turner, A. Dosseto, N. J. Pearson, and C. Beier (2008), Source depletion and extent of melting in the Tongan sub-arc mantle, *Earth Planet. Sci. Lett.*, *273*, 279–288, doi:10.1016/j.epsl.2008.06.040.

Cervantes, P., and P. Wallace (2003), Role of H_2O in subduction zone magmatism: New insights from melt inclusions in high-Mg basalts from central Mexico, *Geology*, *31*, 235–238, doi:10.1130/0091-7613(2003)031<0235:ROHOIS>2.0.CO;2.

Cooper, L. B., T. Plank, R. J. Arculus, E. H. Hauri, P. S. Hall, and S. W. Parman (2010), High-Ca boninites from the active Tonga Arc, *J. Geophys. Res.*, *115*, B10206, doi:10.1029/2009JB006367.

Currie, C. A., C. Beaumont, and R. S. Huismans (2007), The fate of subducted sediments: A case for backarc intrusion and underplating, *Geology*, *35*, 1111–1114, doi:10.1130/G24098A.1.

Davies, J. H., and D. J. Stevenson (1992), Physical model of source region subduction zone volcanics, *J. Geophys. Res.*, *97*, 2037–2070, doi:10.1029/91JB02571.

Defant, M. J., and M. S. Drummond (1990), Derivation of some modern arc magmas by melting of young subducted lithosphere, *Nature*, *347*, 662–665, doi:10.1038/347662a0.

Dixon, J. E., and D. A. Clague (2001), Volatiles in basaltic glasses from Loihi Seamount, Hawaii: Evidence for a relatively dry plume component, *J. Petrol.*, *42*, 627–654, doi:10.1093/petrology/42.3.627.

Dixon, J. E., L. Leist, C. Langmuir, and J. G. Schilling (2002), Recycled dehydrated lithosphere observed in plume-influenced mid-ocean ridge basalt, *Nature*, *420*, 385–389, doi:10.1038/nature01215.

Eiler, J. M., A. Crawford, T. Elliott, K. A. Farley, J. W. Valley, and E. M. Stolper (2000), Oxygen isotope geochemistry of oceanic arc lavas, *J. Petrol.*, *41*, 229–256, doi:10.1093/petrology/41.2.229.

Eiler, J. M., M. J. Carr, M. Reagan, and E. Stolper (2005), Oxygen isotope constraints on the sources of Central American arc lavas, *Geochem. Geophys. Geosyst.*, *6*, Q07007, doi:10.1029/2004GC000804.

Elliott, T. (2003), Tracers of the slab, in *Inside the Subduction Factory*, *Geophys. Monogr. Ser.*, vol. 138, edited by J. Eiler, pp. 23–45, AGU, Washington, D. C., doi:10.1029/138GM03.

Elliott, T. R., T. Plank, A. Zindler, W. White, and B. Bourbon (1997), Element transport from slab to volcanic front at the Mariana Arc, *J. Geophys. Res.*, *102*, 14,991–15,019, doi:10.1029/97JB00788.

England, P. C., and R. F. Katz (2010), Melting above the anhydrous solidus controls the location of volcanic arcs, *Nature*, *467*, 700–703, doi:10.1038/nature09417.

England, P., and C. A. Wilkins (2004), Simple Analytical Approximation to the Temperature Structure in Subduction Zones, *Geophys. J. Int.*, *159*, 1138–1154, doi:10.1111/j.1365-246X.2004.02419.x.

England, P., R. Engdahl, and W. Thatcher (2004), Systematic variation in the depths of slabs beneath arc volcanoes, *Geophys. J. Int.*, *156*(2), 377–408, doi:10.1111/j.1365-246X.2003.02132.x.

George, R., S. Turner, J. Morris, T. Plank, C. Hawkesworth, and J. Ryan (2005), Pressure-temperature-time paths of sediment recycling beneath the Tonga-Kermadec arc, *Earth Planet. Sci. Lett.*, *233*, 195–211, doi:10.1016/j.epsl.2005.01.020.

Gerya, T. V., and B. Stoeckhert (2006), 2-D numerical modeling of tectonic and metamorphic histories at active continental margins, *Int. J. Earth Sci.*, *95*, 250–274, doi:10.1007/s00531-005-0035-9.

Gerya, T. V., and D. A. Yuen (2003), Rayleigh-Taylor instabilities from hydration and melting propel "cold plumes" at subduction zones, *Earth Planet. Sci. Lett.*, *212*, 47–62, doi:10.1016/S0012-821X(03)00265-6.

Gerya, T. V., B. Stoeckhert, and A. L. Perchuk (2002), Exhumation of high-pressure metamorphic rocks in a subduction channel: A numerical simulation, *Tectonics*, *21*(6), 1056, doi:10.1029/2002TC001406.

Grove, T. L., S. W. Parman, S. A. Bowring, R. C. Price, and M. B. Baker (2002), The role of an H_2O-rich fluid component in the generation of primitive basaltic andesites and andesites from the Mt. Shasta region, N. California, *Contrib. Mineral. Petrol.*, *142*, 375–396, doi:10.1007/s004100100299.

Grove, T. L., C. B. Till, E. Lev, N. Chatterjee, and E. Medard (2009), Kinematic variables and water transport control the formation and location of arc volcanoes, *Nature*, *459*, 694–697, doi:10.1038/nature08044.

Hacker, B. R. (2008), H_2O subduction beneath arcs, *Geochem. Geophys. Geosyst.*, *9*, Q03001, doi:10.1029/2007GC001707.

Hauri, E. H., G. A. Gaetani, and T. H. Green (2006), Partitioning of water during melting of the Earth's upper mantle at H_2O-undersaturated conditions, *Earth Planet. Sci. Lett.*, *248*(3–4), 715–734, doi:10.1016/j.epsl.2006.06.014.

Hayden, L. A., and C. E. Manning (2011), Rutile solubility in supercritical $NaAlSi_3O_8$-H_2O fluids, *Chem. Geol.*, *284*, 74–81, doi:10.1016/j.chemgeo.2011.02.008.

Hayden, L. A., and E. B. Watson (2007), A diffusion mechanism for core-mantle interaction, *Nature*, *450*, 709–711, doi:10.1038/nature06380.

Hebert, L. B., and M. C. Gurnis (2010) Geophysical Implications of Izu-Bonin mantle wedge hydration from chemical geodynamic modeling, *Isl. Arc*, *19*, 134–150, doi:10.1111/j.1440-1738.2009.00688.x.

Hebert, L. B., P. Antoshechkina, P. D. Asimow, and M. C. Gurnis (2009) Emergence of a low- viscosity channel in subduction zones through the coupling of mantle flow and thermodynamics, *Earth Planet. Sci. Lett.*, *278*, 243–256, doi: 10.1016/j.epsl.2008.12.013.

Hermann, J., and D. Rubatto (2009), Accessory phase control on the trace element signature of sediment melts in subduction zones, *Chem. Geol.*, *265*, 512–526, doi:10.1016/j.chemgeo.2009.05.018.

Hermann, J., and C. Spandler (2008), Sediment melts at sub-arc depths: An experimental study, *J. Petrol.*, *49*, 717–740, doi:10.1093/petrology/egm073.

Hermann, J., C. Spandler, A. Hack, and A. V. Korsakov (2006), Aqueous fluids and hydrous melts in high-pressure and ultra-high pressure rocks: Implications for element transfer in subduction zones, *Lithos*, *92*, 399–417, doi:10.1016/j.lithos.2006.03.055.

Hirschmann, M. M., A. C. Withers, and C. Aubaud (2006), Petrologic structure of a hydrous 410 km discontinuity, in *Earth's Deep Water Cycle*, *Geophys. Monogr. Ser.*, vol. 168, edited by S. D. Jacobsen and S. van der Lee pp. 277–287, AGU, Washington, D. C., doi:10.1029/168GM21.

Iwamori, H. (2007), Transportation of H_2O beneath the Japan arcs and its implications for global water circulation, *Chem. Geol.*, *239*, 182–198, doi:10.1016/j.chemgeo.2006.08.011.

Johnson, E. R., P. J. Wallace, H. Delgado Granados, V. C. Manea, A. J. R. Kent, I. N. Bindeman, and C. S. Donegan (2009), Subduction-related volatile recycling and magma generation beneath Central Mexico: Insights from melt inclusions, oxygen isotopes and geodynamic models, *J. Petrol.*, *50*, 1729–1764, doi:10.1093/petrology/egp051.

Johnson, M. C., and T. Plank (1999), Dehydration and melting experiments constrain the fate of subducted sediments, *Geochem. Geophys. Geosyst.*, *1(*12), 1007, doi:10.1029/1999GC000014.

Kay, S. M., R. W. Kay, and G. P. Citron (1982), Tectonic controls on tholeiitic and calc-alkaline magmatism in the Aleutian Arc, *J. Geophys. Res.*, *87*, 4051–4072, doi:10.1029/JB087iB05p04051.

Kelemen, P. B., J. L. Rilling, E. M. Parmentier, L. Mehl, and B. R. Hacker (2003), Thermal structure due to solid-state flow in the mantle wedge beneath arcs, in *Inside the Subduction Factory*, *Geophys. Monogr. Ser.*, vol. 138, edited by J. Eiler, pp. 293–311, AGU, Washington, D. C., doi:10.1029/138GM13.

Keppler, H. (1996), Constraints from partitioning experiments on the composition of subduction-zone fluids, *Nature*, *380*, 237–240, doi:10.1038/380237a0.

Kessel, R., M. W. Schmidt, T. Pettke, and P. Ulmer (2005a), The trace element signature of subduction zone fluids, melts, and supercritical liquids at 120–180 km depth, *Nature*, *437*, 724–727, doi:10.1038/nature03971.

Kessel, R., P. Ulmer, T. Pettke, M. W. Schmidt, and A. B. Thompson (2005b), The water-basalt system at 4 to 6 GPa: Phase relations and second critical endpoint in a K-free eclogite at 700 to 1400°C, *Earth Planet. Sci. Lett.*, *237*, 873–892, doi:10.1016/j.epsl.2005b.06.018.

Kincaid, C., and R. W. Griffiths (2004), Variability in flow and temperatures within mantle subduction zones, *Geochem. Geophys. Geosyst.*, *5*, Q06002, doi:10.1029/2003GC000666.

Kincaid, C., and I. S. Sacks (1997), Thermal and dynamical evolution of the upper mantle in subduction zones, *J. Geophys. Res.*, *102*(B6), 12,295–12,315, doi:10.1029/96JB03553.

King, R. L., G. E. Bebout, T. Moriguti, and E. Nakamura (2006), Elemental mixing systematics and Sr-Nd isotope geochemistry of melange formation: Obstacles to identification of fluid sources to arc volcanics, *Earth Planet. Sci. Lett.*, *246*, 288–304, doi:10.1016/j.epsl.2006.03.053.

Klimm, K., J. D. Blundy, and T. H. Green (2008), Trace element partitioning and accessory phase saturation during H_2O-saturated melting of basalt with implications for subduction zone chemical fluxes, *J. Petrol.*, *49*(3), 523–553, doi:10.1093/petrology/egn001.

Kneller, E. A., and P. E. van Keken (2008), The effects of three-dimensional slab geometry on deformation in the mantle wedge: Implications for shear wave anisotropy, *Geochem. Geophys. Geosyst.*, *9*, Q01003, doi:10.1029/2007GC001677.

Leeman, W. P., J. P. Lewis, R. C. Evarts, R. M. Conrey, and M. J. Streck (2005), Petrologic constraints on the thermal structure of the southern Washington Cascades, *J. Volcanol. Geotherm. Res.*, *140*, 67–105, doi:10.1016/j.jvolgeores.2004.07.016.

MacKenzie, L. S., G. A. Abers, K. M. Fischer, E. M. Syracuse, J. M. Protti, V. Gonzalez, and W. Strauch (2008), Crustal structure along the southern Central American volcanic front, *Geochem. Geophys. Geosyst.*, *9*, Q08S09, doi:10.1029/2008GC001991.

Manning, C. E. (2004), The chemistry of subduction-zone fluids, *Earth Planet. Sci. Lett.*, *223*, 1–16, doi:10.1016/j.epsl.2004.04.030.

Martin, E., I. Bindeman, and T. L. Grove (2011), The origin of high-Mg magmas in Mt Shasta and Medicine Lake volcanoes, Cascade Arc (California): Higher and lower than mantle oxygen isotope signatures attributed to current and past subduction, *Contrib. Mineral. Petrol.*, *162*, 945–960, doi:10.1007/s00410-011-0633-4.

McDade, P., J. Blundy, and B. J. Wood (2003), Trace element partitioning on the Tinaquillo lherzolite solidus at 1.5 GPa, *Phys. Earth Planet. Inter.*, *139*, 129–147, doi:10.1016/S0031-9201(03)00149-3.

Mibe, K., T. Kawamoto, K. N. Matsukage, Y. Fei, and S. Ono (2011), Slab melting versus slab dehydration in subduction-zone magmatism, *Proc. Natl. Acad. Sci. U. S. A.*, *108*, 8177–8182, doi:10.1073/pnas.1010968108.

Michael, P. J. (1995), Regionally distinctive sources of depleted MORB; Evidence from trace elements and H_2O, *Earth Planet. Sci. Lett.*, *131*, 301–320, doi:10.1016/0012-821X(95)00023-6.

Montel, J.-M. (1993), A model for monazite/melt equilibrium and application to the generation of granitic magmas, *Chem. Geol.*, *110*, 127–146, doi:10.1016/0009-2541(93)90250-M.

Newman, S., E. M. Stolper, and R. J. Stern (2000), H_2O and CO_2 in magmas from Mariana arc and back arc systems, *Geochem. Geophys. Geosyst.*, *1*(5), 1013, doi:10.1029/1999GC000027.

Ohtani, E., K. D. Litasov, T. Hosoya, T. Kubo, and T. Kondo (2004), Water transport into the deep mantle and formation of a hydrous transition zone, *Phys. Earth Planet. Inter.*, *143–144*, 255–269, doi:10.1016/j.pepi.2003.09.015.

Pan, Y., and M. E. Fleet (1996), Rare element mobility during prograde granulite facies metamorphism: Significance of fluorine, *Contrib. Mineral. Petrol.*, *123*, 251–262, doi:10.1007/s004100050154.

Pearce, J. A. (2005), Mantle preconditioning by melt extraction during flow: Theory and petrogenetic implications, *J. Petrol.*, *46*, 973–997, doi:10.1093/petrology/egi007.

Pearce, J. A., R. J. Stern, S. H. Bloomer, and P. Fryer (2005), Geochemical mapping of the Mariana arc-basin system: Implications for the nature and distribution of subduction components, *Geochem. Geophys. Geosyst.*, *6*, Q07006, doi:10.1029/2004GC000895.

Plank, T. (2005), Constraints from Th/La sediment recycling at subduction zones and the evolution of the continents, *J. Petrol.*, *46*(5), 921–944, doi:10.1093/petrology/egi005.

Plank, T., L. B. Cooper, and C. E. Manning (2009), Emerging geothermometers for estimating slab surface temperatures, *Nat. Geosci.*, *2*, 611–615, doi:10.1038/ngeo614.

Portnyagin, M., K. Hoernle, P. Plechov, N. Mironov, and S. Khubunaya (2007), Constraints on mantle melting and composition and nature of slab components in volcanic arcs from volatiles (H_2O, S, Cl, F) and trace elements in melt inclusions from the Kamchatka Arc, *Earth Planet. Sci. Lett.*, *255*(1–2), 53–69, doi:10.1016/j.epsl.2006.12.005.

Reiners, P. W., P. E. Hammond, J. M. McKenna, and R. A. Duncan (2000), Young basalts of the central Washington Cascades, flux melting of the mantle, and geochemical

signatures of primitive arc magmas, *Contrib. Mineral. Petrol.*, *138*, 249–264, doi:10.1007/s004100050561.

Rowe, M. C., A. J. R. Kent, and R. L. Nielsen (2009), Subduction influence on oxygen fugacity and trace and volatile elements in basalts across the Cascades volcanic arc, *J. Petrol.*, *50*, 61–91, doi:10.1093/petrology/egn072.

Rüpke, L. H., J. Phipps Morgan, M. Hort, and J. Connolly (2002), Are the regional variations in Central American arc lavas dues to different basaltic versus peridotitic slab sources of fluids?, *Geology*, *30*, 1035–1038, doi:10.1130/0091-7613(2002)030<1035:ATRVIC>2.0.CO;2.

Ruscitto, D. M., P. J. Wallace, E. R. Johnson, A. J. R. Kent, and I. N. Bindeman (2010), Volatile contents of mafic magmas from cinder cones in the Central Oregon High Cascades: Implications for magma formation and mantle conditions in a hot arc, *Earth Planet. Sci. Lett.*, *298*, 153–161, doi:10.1016/j.epsl.2010.07.037.

Ruscitto, D. M., P. J. Wallace, and A. J. R. Kent (2011), Revisiting the compositions and volatile contents of olivine-hosted melt inclusions from the Mount Shasta region: Implications for the formation of high-Mg andesites, *Contrib. Mineral. Petrol.*, *162*, 109–132, doi:10.1007/s00410-010-0587-y.

Ruscitto, D. M., P. J. Wallace, L. B. Cooper, and T. Plank (2012), Global variations in H_2O/Ce: 2. Relationships to arc magma geochemistry and volatile fluxes, *Geochem. Geophys. Geosyst.*, *13*, Q03025, doi:10.1029/2011GC003887.

Schmidt, M. W., and S. Poli (1998), Experimentally based water budgets for dehydrating slabs and consequences for arc magma generation, *Earth Planet. Sci. Lett.*, *163*, 361–379, doi:10.1016/S0012-821X(98)00142-3.

Schmidt, M. W., A. Dardon, G. Chazot, and R. Vannucci (2004), Rutile—Melt partitioning of Nb and Ta dependent on melt composition and Nb/Ta fractionation in the Earth, *Earth Planet. Sci. Lett.*, *226*, 415–432, doi:10.1016/j.epsl.2004.08.010.

Simons, K., J. Dixon, J.-G. Schilling, R. Kingsley, and R. Poreda (2002), Volatiles in basaltic glasses from the Easter-Salas y Gomez Seamount Chain and Easter Microplate: Implications for geochemical cycling of volatile elements, *Geochem. Geophys. Geosyst.*, *3*(7), 1039, doi:10.1029/2001GC000173.

Skora, S. E., and J. D. Blundy (2010a), High-pressure hydrous phase relations of radiolarian clay and implications for the involvement of subducted sediment in arc magmatism, *J. Petrol.*, *51*, 2211–2243, doi:10.1093/petrology/egq054.

Skora, S. E., and J. D. Blundy (2010b) Monazite saturation in silicate melts at high pressure with implications for subduction zone volcanism, Abstract V12B-03 presented at 2010 Fall Meeting, AGU, San Francisco, Calif., 13–17 Dec.

Sobolev, A. V., and M. Chaussidon (1996), H_2O concentrations in primary melts from suprasubduction zones and mid-ocean ridges; implications for H_2O storage and recycling in the mantle, *Earth Planet. Sci. Lett.*, *137*(1–4), 45–55, doi:10.1016/0012-821X(95)00203-O.

Spiegelman, M., P. E. van Keken, and B. Hacker (2008) Volatiles and melting: Advanced models of fluid flow in subduction systems, *Eos Trans. AGU*, *89*(53), Fall Meet. Suppl., Abstract U53A-0064.

Stolper, E., and S. Newman (1994), The role of water in the petrogenesis of Mariana trough magmas, *Earth Planet. Sci. Lett.*, *121*, 293–325, doi:10.1016/0012-821X(94)90074-4.

Straub, S. M., G. D. Layne, A. Schmidt, and C. H. Langmuir (2004), Volcanic glasses at the Izu arc volcanic front: New perspectives on fluid and sediment melt recycling in subduction zones, *Geochem. Geophys. Geosyst.*, *5*, Q01007, doi:10.1029/2002GC000408.

Sun, S., and W. F. McDonough (1989), Chemical and isotopic systematics of oceanic basalts: implications for mantle composition and processes, in *Magmatism in the Ocean Basins*, edited by A. D. Saunders and M. J. Norry, *Spec. Publ. Geol. Soc.*, *42*, 313–345.

Syracuse, E. M., and G. A. Abers (2006), Global compilation of variations in slab depth beneath arc volcanoes and implications, *Geochem. Geophys. Geosyst.*, *7*, Q05017, doi:10.1029/2005GC001045.

Syracuse, E. M., G. A. Abers, K. Fischer, L. MacKenzie, C. Rychert, M. Protti, V. González, and W. Strauch (2008), Seismic tomography and earthquake locations in the Nicaraguan and Costa Rican upper mantle, *Geochem. Geophys. Geosyst.*, *9*, Q07S08, doi:10.1029/2008GC001963.

Syracuse, E. M., P. E. van Keken, and G. A. Abers (2010), The global range of subduction zone thermal models, *Phys. Earth Planet. Inter.*, *183*(1–2), 73–90, doi:10.1016/j.pepi.2010.02.004.

Tatsumi, Y. (1986), Formation of the volcanic front in subduction zones, *Geophys. Res. Lett.*, *13*, 717–720, doi:10.1029/GL013i008p00717.

Thomsen, T. B., and M. W. Schmidt (2008), Melting of carbonated pelites at 2.5–5.0 GPa, silicate- carbonatite liquid immiscibility, and potassium-carbon metasomatism of the mantle, *Earth Planet. Sci. Lett.*, *267*, 17–31, doi:10.1016/j.epsl.2007.11.027.

Till, R. (1974), Correlation and regression, in *Statistical Methods for Earth Scientists: An Introduction*, chap. 5, pp. 83–103, John Wiley, New York.

Tropper, P., C. E. Manning, and D. Harlov (2011), Solubility of $CePO_4$ monazite and YPO_4 xenotime in H_2O and H_2O-NaCl at 800°C and 1 GPa: Implications for REE and Y transport during high-grade metamorphism, *Chem. Geol.*, *282*, 58–66, doi:10.1016/j.chemgeo.2011.01.009.

Tsuno, K., and R. Dasgupta (2012), The effect of carbonates on near-solidus melting of pelite at 3 GPa: Relative efficiency of H_2O and CO_2 subduction, *Earth Planet. Sci. Lett.*, *319–320*, 185–196, doi:10.1016/j.epsl.2011.12.007.

Turner, S., C. Hawkesworth, R. Macdonald, S. Black, and P. van Calsteren (1996), U-series isotopes and destructive plate margin magma genesis in the Lesser Antilles, *Earth Planet. Sci. Lett.*, *142*, 191–207, doi:10.1016/0012-821X(96)00078-7.

van Keken, P. E., B. Kiefer, and S. M. Peacock (2002), High resolution models of subduction zones: Implications for mineral dehydration reactions and the transport of water into the deep mantle, *Geochem. Geophys. Geosyst.*, *3*(10), 1056, doi:10.1029/2001GC000256.

van Keken, P. E., B. R. Hacker, E. M. Syracuse, and G. A. Abers (2011), Subduction factory: 4. Depth-dependent flux of H_2O from subducting slabs worldwide, *J. Geophys. Res.*, *116*, B01401, doi:10.1029/2010JB007922.

Vielzeuf, D., and M. W. Schmidt (2001), Melting relations in hydrous systems revisited: Application to metapelites, metagreywackes and metabasalts, *Contrib. Mineral. Petrol.*, *141*, 251–267, doi:10.1007/s004100100237.

Wada, I., and K. Wang (2009), Common depth of decoupling between the subducting slab and mantle wedge: Reconciling diversity and uniformity of subduction zones, *Geochem. Geophys. Geosyst.*, *10*, Q10009, doi:10.1029/2009GC002570.

Wallace, P. J. (2005), Volatiles in subduction zone magmas; concentrations and fluxes based on melt inclusion and volcanic

gas data, *J. Volcanol. Geotherm. Res.*, *140*(1–3), 217–240, doi:10.1016/j.jvolgeores.2004.07.023.

Workman, R. K., and S. R. Hart (2005), Major and trace element composition of the depleted MORB mantle (DMM), *Earth Planet. Sci. Lett.*, *231*, 53–72, doi:10.1016/j.epsl.2004.12.005.

Workman, R. K., E. Hauri, S. R. Hart, J. Wang, and J. Blusztajn (2006), Volatile and trace elements in basaltic glasses from Samoa: Implications for water distribution in the mantle, *Earth Planet. Sci. Lett.*, *241*, 932–951, doi:10.1016/j.epsl.2005.10.028.

Zimmer, M. M., T. Plank, E. H. Hauri, G. M. Yogodzinski, P. Stelling, J. Larsen, B. Singer, B. Jicha, C. Mandeville, and C. J. Nye (2010), The role of water in generating the calc-alkaline trend: New volatile data for aleutian magmas and a new Tholeiitic Index, *J. Petrol.*, *51*, 2411–2444, doi:10.1093/petrology/egq062.

Supplement A: Data Sources and Treatment

Olivine-hosted melt inclusions (MIs) were corrected for post-entrapment crystallization following the procedures in each study. Plagioclase- and pyroxene-hosted MIs were not corrected for post-entrapment crystallization. To limit the effects of magmatic differentiation, all MI and whole rock (WR) compositions were screened for SiO_2 <57 wt. % (normalized to 100%, with all Fe as FeO). To limit the effects of magmatic degassing, all MIs were screened for S >500 ppm.

Least-degassed H_2O contents were obtained from the MIs containing the maximum H_2O content from each volcano (measured by SIMS or FTIR). Trace element (TE) compositions were obtained from either the WR-host of the least-degassed MI (preferred; measured mostly by high-precision ICP-MS), the average of several WRs from the same volcano, the least-degassed MI (measured by SIMS or LA-ICP-MS), or the average of several MIs from the same sample. K_2O was obtained from the least-degassed MI (measured by EMP; calculated hydrous, with all Fe as FeO).

Tonga

MIs: *Cooper et al.*, 2009 (Volcanoes 19, 7, Tofua, D, F, L); Cooper et al., 2010 (Volcano A)
WRs: *Cooper et al.*, 2009 (Volcanoes 19, 7, D, F, L); *Caulfield et al.*, submitted (in press); *Cooper et al.*, 2010 (Volcano A)
Notes: TEs are from the WR-hosts.

Marianas

MIs: *Kelley et al.*, 2010 (Sarigan, Guguan, Pagan, Agrigan)
WRs: *Woodhead et al.*, 2001 and *Elliott et al.*, 1997 (Sarigan); *Kelley et al.*, 2010 (Guguan, Pagan, Agrigan);
Notes: TEs are from the WR-hosts, except for Sarigan (average of several WRs).

Kamchatka

MIs and WRs: *Portnyagin et al.*, 2007 (Chikurachki, Ksudach, Karymsky, Tolbachik); *Auer et al.*, 2009 (Klyuchevskoy)

Notes: TEs are from least-degassed MIs, except for Tolbachik (average of several MIs from the same sample) and Klyuchevskoy (WR-host).

Aleutians

MIs: *Zimmer et al.*, 2010 (Korovin, Seguam, Okmok, Pakushin, Akutan, Shishaldin, Emmons, Augustine)

WRs: *Zimmer*, 2008 (Korovin, Seguam, Okmok, Pakushin, Akutan, Shishaldin, Emmons, Augustine)

Notes: TEs are from the WR-hosts, except for Akutan and Emmons (average of several WRs), and Augustine (another WR).

Cascadia

MIs and WRs: *Ruscitto et al.*, 2010 (Blue Lake, Garrison Butte, Twin Craters, Yapoah, Island Fissure, Collier); *Ruscitto et al.*, 2011 (Shasta);

Notes: TEs are from the WR-hosts, except Blue Lake (several WRs), Island Fissure (average of several MIs from the same sample), and Shasta (least-degassed MI).

Mexico

MIs and WRs: *Johnson et al.*, 2009 (San Juan, Astillero, Hungaro, Paricutin, Jorullo); *Cervantes and Wallace*, 2003 (Jumiltepec, Las Tetillas, Tuxtepec, Tepetlapa);

Notes: TEs are from the WR-hosts, except Paricutin (least-degassed MI).

Guatemala

MIs: *Sadofsky et al.*, 2008; *Wehrmann et al.*, 2011 (Santa Maria, Atitlan, Fuego, Agua)

Notes: TEs are from the least-degassed MIs, excluding Santa Maria (another MI from the same sample).

Nicaragua

MIs: *Sadofsky et al.*, 2008; *Wehrmann et al.*, 2011 (Cerro Negro, Nejapa, Granada)

Notes: TEs are from the least-degassed MIs.

Costa Rica

MIs and WRs: *Wade et al.*, 2006 (Arenal); *Benjamin et al.*, 2007 (Irazu)

Notes: TEs are from the WR-hosts.

Lesser Antilles

MIs: *Bouvier et al.*, 2008 (St. Vincent); *Bouvier et al.*, 2010 (St. Vincent)

Notes: TEs from St. Vincent are from the least-degassed MI. We were unable to include data from Grenada from *Bouvier et al.* [2010a], due to the very large and unsystematic variation in the Nb/Ce melt inclusion data reported by *Bouvier et al.* [2010b] and whole rock data reported by *Shimuzu and Arculus* [1975], *Thirlwall et al.* [1996], and *Woodland et al.* [2002]. In their analyses, Nb/Ce varies from ~0.1 to >1.0 in melt inclusions from a single sample, while Nb/Ce varies from <0.1 to ~0.6 in the WRs. This is a greater variation than the entire global dataset. No whole rock analysis was reported for the melt inclusion host volcanic.

References

Auer, S., I. Bindeman, P. Wallace, Vera Ponomareva, and M. Portnyagin (2009), The origin of hydrous, high-d^{18}O voluminous volcanism: diverse oxygen isotope values and high magmatic water contents within the volcanic record of Klyuchevskoy volcano, Kamchatka, Russia, *Contrib. Mineral. Petrol.*, *157*, 209–230, doi:10.1007/s00410-008-0330-0.

Benjamin, E.R., T. Plank, J.A. Wade, K.A. Kelley, E.H. Hauri, and G.E. Alvarado (2007), High water contents in basaltic magmas from Irazú Volcano, Costa Rica, *J. Volcanol. Geoth. Res., 168*, 68-92, doi:10.1016/j.jvolgeores.2007.08.008.

Bouvier, A.-S., N. Métrich, and E. Deloule, (2008), Slab-Derived Fluids in the Magma Sources of St. Vincent (Lesser Antilles Arc): Volatile and Light Element Imprints, *J. Petrol.*, *49*, 1427-1448, doi:10.1093/petrology/egn031.

Bouvier, A.-S., N. Métrich, and E. Deloule (2010a), Light elements, volatiles, and stable isotopes in basaltic melt inclusions from Grenada, Lesser Antilles: Inferences for magma genesis, Geochem. Geophys. Geosyst.,11, Q09004, doi:10.1029/2010GC003051.

Bouvier, A.-S., E. Deloule, and N. Métrich (2010b), Fluid Inputs to Magma Sources of St. Vincent and Grenada (Lesser Antilles): New Insights from Trace Elements in Olivine-hosted Melt Inclusions, *J. Petrol.*, *51*, 1597-1615, doi:10.1093/petrology/egq031.

Caulfield, J.T., S.P. Turner, I.E.M. Smith, L.B. Cooper, and G.A. Jenner (2012), Magma evolution in the primitive, intra-oceanic Tonga arc. I Petrogenesis of basaltic andesites at Tofua Volcano, *J. Petrol.*, in press.

Cervantes P., and P. Wallace (2003), Role of H_2O in subduction zone magmatism: New insights from melt inclusions in high-Mg basalts from central Mexico, *Geology*, *31*, 235-238, doi: 10.1130/0091-7613(2003)031<0235:ROHOIS>2.0.CO;2.

Cooper, L.B. (2009), Volatiles in Tonga Arc magmas and their role in unraveling subduction zone processes, Ph.D. thesis, Dep. of Earth Sciences, Boston University, Boston, Massachusetts, USA.

Cooper, L.B., T. Plank, R.J. Arculus, E.H. Hauri, P.S. Hall, and S.W. Parman (2010), High-Ca boninites from the active Tonga Arc, *J. Geophys. Res.*, *115*, B10206, doi:10.1029/2009JB006367.

Elliott, T.R., T. Plank, A. Zindler, W. White, and B. Bourbon (1997), Element transport from slab to volcanic front at the Mariana Arc, *J. Geophys. Res*, *102*, 14991-15019.

Johnson, E.R., P.J. Wallace, H. Delgado Granados, V.C. Manea, A.J.R. Kent, I.N. Bindeman, C.S. Donegan (2009), Subduction-related volatile recycling and magma generation beneath Central Mexico: insights from melt inclusions, oxygen isotopes and geodynamic models, *J. Petrol.*, *50*, 1729–1764, doi: 10.1093/petrology/egp051.

Kelley, K.A., T. Plank, S. Newman, E.M. Stolper, T.L. Grove, S. Parman, and E.H. Hauri (2010), Mantle melting as a function of water content beneath the Mariana arc, *J. Petrol.*, *51(8)*, 1711-1738, doi:10.1093/petrology/egq036.

Portnyagin, M., K. Hoernle, P. Plechov, N. Mironov, and S. Khubunaya (2007), Constraints on mantle melting and composition and nature of slab components in volcanic arcs from volatiles (H_2O, S, Cl, F) and trace elements in melt inclusions from the Kamchatka Arc, *Earth Planet. Sci. Lett., 255*(1-2),53-69, doi:10.1016/j.epsl.2006.12.005.

Ruscitto, D.M., P.J. Wallace, E.R. Johnson, A.J.R. Kent, and I.N. Bindeman (2010), Volatile contents of mafic magmas from cinder cones in the Central Oregon High Cascades: implications for magma formation and mantle conditions in a hot arc, *Earth Planet. Sci. Lett.*, *298*, 153-161, doi:10.1016/j.epsl.2010.07.037.

Ruscitto, D.M., P.J. Wallace, and A.J.R. Kent (2011), Revisiting the compositions and volatile contents of olivine-hosted melt inclusions from the Mount Shasta region: implications for the formation of high-Mg andesites, *Contrib. Mineral. Petrol.*, *162*, 109-132, doi:10.1007/s00410-010-0587-y.

Sadofsky, S.J., M. Portnyagin, K. Hoernle, and P. van den Bogaard (2008), Subduction cycling of volatiles and trace elements through the Central American volcanic arc: evidence from melt inclusions, *Contrib. Mineral. Petrol., 155*, 433-456, doi:10.1007/s00410-007-0251-3.

Shimizu, N. and R.J. Arculus (1975), Rare earth element concentrations in a suite of basanitoids and alkali olivine basalts from Grenada, Lesser Antilles, *Contrib. Mineral. Petrol.*, 50, 231-240.

Thirlwall, M.F., A.M. Graham, R.J. Arculus, R.S. Harmon, and C.G. Macpherson (1996), Resolution of the effects of crustal contamination, sediment subduction, and fluid transport in island arc magmas: Pb-Sr-Nd-O isotope geochemistry of Grenada, Lesser Antilles, *Geochim. Cosmochim. Ac.*, *60*, 4785-4810.

Wade, J.A., T. Plank, W.G. Melson, G.J. Soto, and E.H. Hauri (2006), The volatile content of magmas from Arenal volcano, Costa Rica, *J. Volcanol. Geotherm. Res.*, *157*, 94-120, doi:10.1016/j.jvolgeores.2006.03.045.

Wehrmann, H., K. Hoernle, M. Portnyagin, M. Wiedenbeck, K. Heydolph (2011) Volcanic CO_2 output at the Central American subduction zone inferred from melt inclusions in olivine crystals from mafic tephras, *Geochem. Geophys. Geosyst.*,*12*, Q06003, doi:10.1029/2010GC003412.

Woodhead, J.D., J.M. Hergt, J.P. Davidson, and S.M. Eggins (2001) Hafnium isotope evidence for 'conservative' element mobility during subduction zone processes, *Earth Planet Sci. Lett.*, *192*, 331-346.

Woodland, S. J., D.G. Pearson, and M.F. Thirlwall (2002), A platinium group element and Re-Os isotope investigation of siderophile element recycling in subduction zone: comparison of Grenada, Lesser Antilles Arc and the Izu-Bonin Arc, *J. Petrol.*, *43*, 171-198.

Zimmer, M.M. (2008), Water in Aleutian magmas: Its origins in the subduction zone and its effects on magma evolution, Ph.D. thesis, Dep. of Earth Sciences, Boston University, Boston, Massachusetts, USA.

Zimmer, M.M., T. Plank, E.H. Hauri, G.M. Yogodzinski, P. Stelling, J. Larsen, B. Singer, B. Jicha, C. Mandeville, and C.J. Nye (2010), The Role of Water in Generating the Calc-alkaline Trend: New Volatile Data for Aleutian Magmas and a New Tholeiitic Index, *J. Petrol.*, *51*, 2411-2444, doi: 10.1093/petrology/egq062.